iScience

CellPress

Article

Detection of a High-Turnover Serotonin Circuit in the Mouse Brain Using Mass Spectrometry Imaging

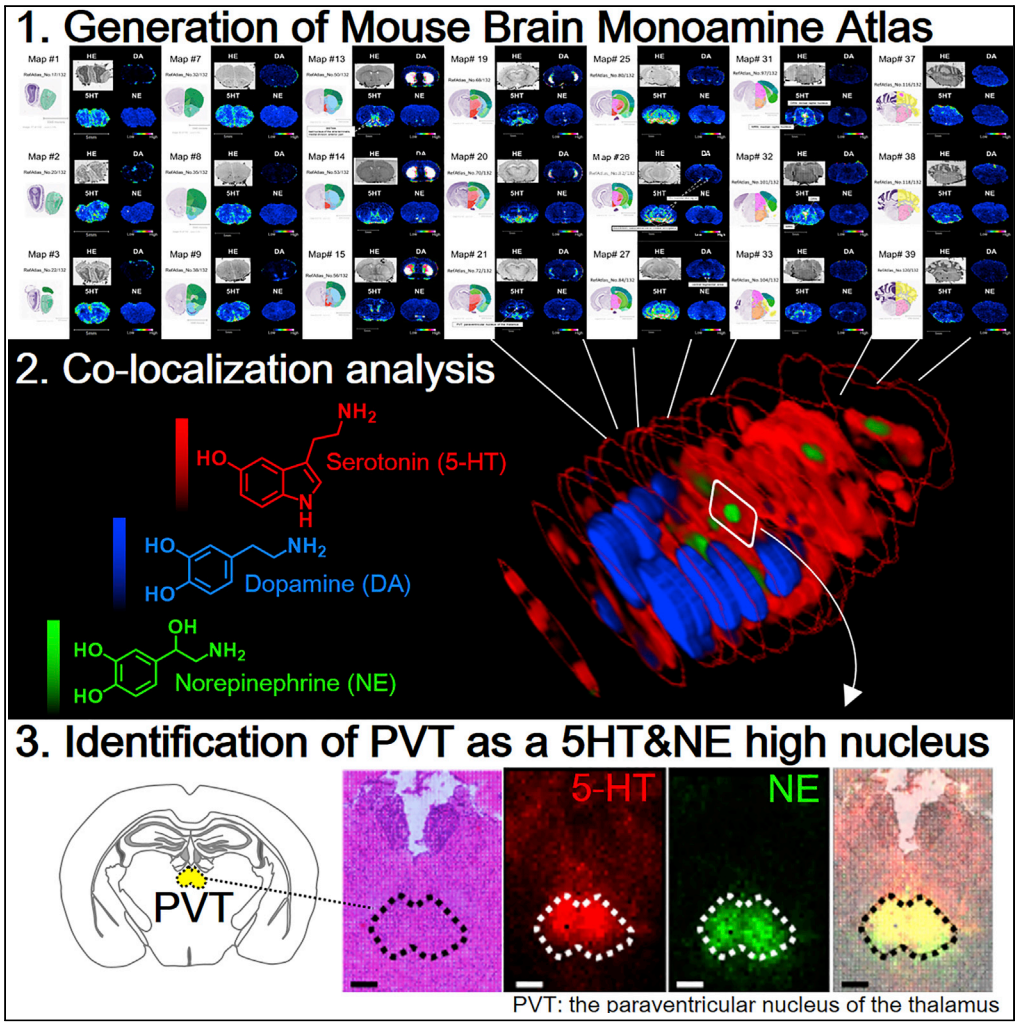

Eiji Sugiyama, Matteo M. Guerrini, Kurara Honda, ..., Sidonia Fagarasan, Makoto Suematsu, Yuki Sugiura

yuki.sgi@keio.jp

HIGHLIGHTS

A murine brain atlas of monoamine (5-HT, DA, NE) levels was generated via MS imaging

We identified several nuclei rich in both 5-HT and a catecholamine (DA or NE)

The paraventricular nucleus of the thalamus (PVT) had high levels of 5-HT and NE

The level of 5-HT in raphe to PVT pathway changed dynamically in response to blood Trp level

Sugiyama et al., iScience *20*, 359–372
October 25, 2019
https://doi.org/10.1016/j.isci.2019.09.036

iScience

CellPress

Article

Detection of a High-Turnover Serotonin Circuit in the Mouse Brain Using Mass Spectrometry Imaging

Eiji Sugiyama,[1] Matteo M. Guerrini,[2] Kurara Honda,[1] Yuko Hattori,[1] Manabu Abe,[3] Patrik Källback,[4,5] Per E. Andrén,[4,5] Kenji F. Tanaka,[6] Mitsutoshi Setou,[7] Sidonia Fagarasan,[2] Makoto Suematsu,[1] and Yuki Sugiura[1,8,*]

SUMMARY

Monoamine neurotransmitters are released by specialized neurons regulating behavioral, motor, and cognitive functions. Although the localization of monoaminergic neurons in the brain is well known, the distribution and kinetics of monoamines remain unclear. Here, we generated a murine brain atlas of serotonin (5-HT), dopamine (DA), and norepinephrine (NE) levels using mass spectrometry imaging (MSI). We found several nuclei rich in both 5-HT and a catecholamine (DA or NE) and identified the paraventricular nucleus of the thalamus (PVT), where 5-HT and NE are co-localized. The analysis of 5-HT fluctuations in response to acute tryptophan depletion and infusion of isotope-labeled tryptophan *in vivo* revealed a close kinetic association between the raphe nuclei, PVT, and amygdala but not the other nuclei. Our findings imply the existence of a highly dynamic 5-HT-mediated raphe to PVT pathway that likely plays a role in the brain monoamine system.

INTRODUCTION

Monoamine neurotransmitters are a family of small molecules that include serotonin (5-hydroxytryptamine, 5-HT), dopamine (DA), and norepinephrine (NE), which are secreted by specific neuronal populations that regulate executive functions (Aston-Jones and Cohen, 2005; Lucki, 1998; Wise, 2004). Considering their essential roles in controlling goal-directed and adaptive behavior, the abundance and localization of monoamine neurotransmitters in the brain must be tightly controlled. The total amount of monoamine neurotransmitters in the brain is determined by the ratio between local synthesis and degradation, since they cannot cross the blood-brain barrier (Hardebo and Owman, 1980). The availability of monoamines to neurons is regulated by synaptic secretion (Gantz et al., 2015; Yuen et al., 2014), volume transmission (Fuxe et al., 2010), and neuronal re-uptake mediated by specific transporters (Bermingham and Blakely, 2016).

The pharmacological or genetic alterations in monoamine neurotransmitter levels can cause changes in behavior, such as impulsiveness (Schweighofer et al., 2008), hypolocomotion (Benazzouz et al., 2014), or the sleep-wake cycle (Singh et al., 2015). Numerous studies have shown that regional monoaminergic tuning directs behavior: that is, the depletion of 5-HT in the basolateral amygdala (BLA) reduces anxiety-like behaviors and weakens fear-associated memory (Johnson et al., 2015); the level of DA in the dorsal striatum is directly correlated to the adaptive changes of locomotion in a mouse model of Parkinson disease (Panigrahi et al., 2015); and reduced NE levels in the BLA increases the occurrence of anxiety-like behavior (McCall et al., 2017). Nevertheless, current data do not validate the actual variation in the local concentration or coexistence of monoamines. In addition, the monoaminergic neurons target multiple brain regions, but the kinetics and magnitude of monoaminergic signaling along different projections are not identified. At present, data regarding the intracerebral localization of 5-HT, DA, and NE remain limited and unclear owing to several long-standing technical limitations inherent to their detection. Thus, we assumed that the direct detection of monoamine levels in the brain may be a powerful and unbiased approach to identify the intensity and kinetics of monoaminergic signaling targeting different brain regions.

We used mass spectrometry imaging (MSI) (Caprioli et al., 1997), which is a technique recently developed for the analysis of the molecular composition of a planar sample with high sensitivity and specificity (Nilsson et al., 2015). Unlike other fluorescence- or radioisotope-based imaging techniques (i.e., the Falck-Hillarp method [Falck and Hillarp, 1959], immunohistochemistry [IHC], or autoradiography [ARG]), MSI does not

[1]Department of Biochemistry, Keio University School of Medicine, 35 Shinanomachi, Shinjuku, Tokyo 160-8582, Japan

[2]Laboratory for Mucosal Immunity, Center for Integrative Medical Sciences, RIKEN Yokohama Institute, Tsurumi Ward, Suehirocho, 1 Chome-7-22, Yokohama, Kanagawa Prefecture 230-0045, Japan

[3]Department of Animal Model Development, Brain Research Institute, Niigata University, 1-757 Asahimachi-dori, Chuo-ku, Niigata 951-8585, Japan

[4]Medical Mass Spectrometry Imaging, Department of Pharmaceutical Biosciences, Uppsala University, Box 591 BMC, 75124 Uppsala, Sweden

[5]Science for Life Laboratory, National Resource for Mass Spectrometry Imaging, Uppsala University, Box 591 BMC, 75124 Uppsala, Sweden

[6]Department of Neuropsychiatry, Keio University School of Medicine, 35 Shinanomachi, Shinjuku, Tokyo 160-8582, Japan

[7]Department of Cellular and Molecular Anatomy and International Mass Imaging Center, Hamamatsu University School of Medicine, 1-20-1 Handayama, Higashi-ku, Hamamatsu, Shizuoka 431-3192, Japan

[8]Lead Contact

*Correspondence: yuki.sgi@keio.jp

https://doi.org/10.1016/j.isci.2019.09.036

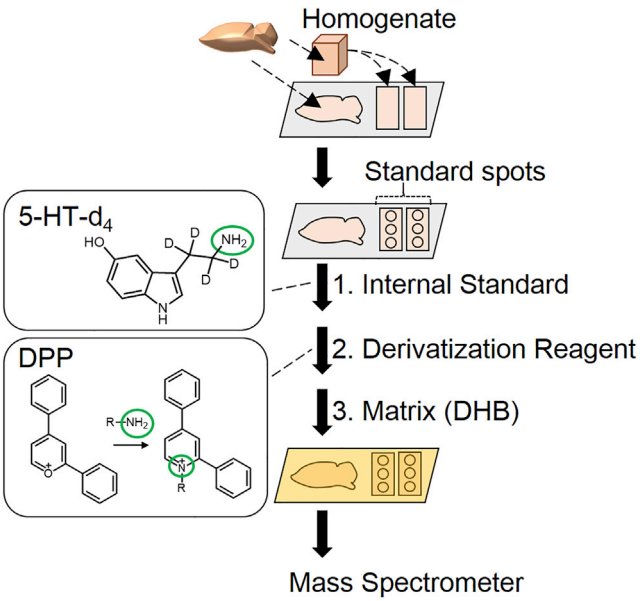

Figure 1. Sample Preparation for Mapping Brain Monoamines Using Mass Spectrometry Imaging

Mouse brain slices and brain homogenate were disposed on conductive glass slides coated with indium-tin-oxide. A series of standard solution containing the known concentration of 5-HT was spotted onto the homogenate sections. An internal standard solution (5 μM of D_4-5-HT in 50% methanol), derivatization solution (1.3 mg/mL of 2,4-diphenyl-pyranylium [DPP] in methanol), and matrix solution (40 mg/mL of 2,5-dihydroxybenzoic acid [DHB] in 50% methanol) were sprayed onto the sections using an automatic sprayer, airbrush, and automatic sprayer, respectively. The DPP derivatives (5-HT-DPP, NE-DPP, and DA-DPP) were detected using mass spectrometers equipped with a MALDI-ion source. See also Transparent Methods and Figure S7.

require any probes and preparations that could affect the distribution of metabolites (i.e., pharmaceutical activation, perfusion, fixation, washing, or blocking); therefore, it is an ideal tool for mapping monoamines in the brain. Although the applicability of MSI had been limited by the low ionization efficacy of monoamines (Shariatgorji et al., 2014; Sugiura et al., 2012), this issue was recently solved with the use of on-tissue chemical derivatization, which converts the primary amino groups of monoamines into quaternary amino groups that provide high ionization efficacy (Shariatgorji et al., 2014). We used 2,4-diphenyl-pyrylium (DPP) since DPP derivatives were detected with better signal intensities than those of other compounds (Esteve et al., 2016; Shariatgorji et al., 2015). We have previously used this approach and detected changes in monoamine levels in the mouse brain (Miyajima et al., 2017; Shariatgorji et al., 2014; Sugiyama et al., 2019).

In this study, we used MSI to generate an atlas of 5-HT, DA, and NE in the whole brain of the C57BL/6J mouse. Our data revealed an unexpected accumulation of multiple monoamines, particularly 5-HT and a catecholamine (DA or NE), in several brain nuclei. Notably, quantitation of 5-HT revealed the paraventricular nucleus of the thalamus (PVT), which receives a raphe-derived dense serotonergic innervation (Migliarini et al., 2013; Muzerelle et al., 2016), as the region containing almost the second highest 5-HT level within the mouse brain. We then analyzed the dynamics of the deprivation and replenishment of 5-HT in specific brain regions following acute tryptophan depletion (ATD) or tryptophan (Trp) supplementation in the mouse diet, which are two treatments known to affect anxiety-like behavior in mice. Our results provided details about monoamine distribution in the brain and the regional differences in 5-HT metabolism and showed that MSI is a powerful system that can be used to detect monoamine fluctuations in the brain of mice subjected to a behavioral experiment.

RESULTS

Generation of a Mouse Brain Atlas of 5-HT, DA, and NE

We analyzed the coronal slices of a mouse brain prepared at an interval of 330 μm (a total of 42 sections) using MSI using an 8-weeks old C57BL/6J male mouse as a representative example (Figure 1). The

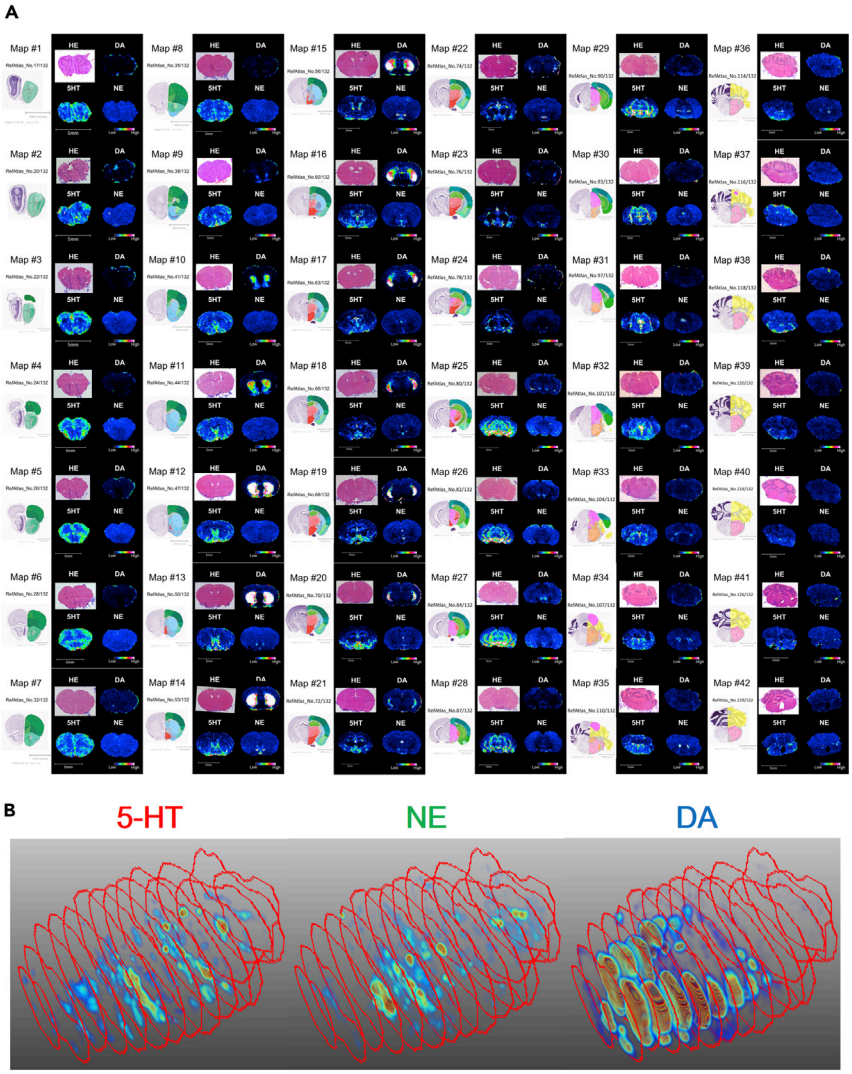

Figure 2. Distribution of 5-HT, NE, and DA in the Mouse Brain

(A) A mouse whole brain atlas of 5-HT, NE, and DA. Hematoxylin and eosin staining and signal intensity of 5-HT, DA, and NE in 42 brain sections of an 8-week-old male C57BL/6J mouse referenced to brain maps from the Allen Brain Reference Atlases (http://atlas.brain-map.org/). Signal intensities were normalized using total ion current and the signal obtained from the slice of the homogenate. The color scales were consistent throughout the series but not between different monoamines. High-resolution images are presented in the Supplemental Information. Data were obtained using a time-of-flight (TOF) mass spectrometer.

(B) Three-dimensional distribution of 5-HT, NE, and DA in the mouse brain. Graphical representation of the normalized signal intensity of 5-HT (left), NE (center), and DA (right) in 15 brain coronal sections of the brain of a C57BL/6J mouse. Red frames represented the shapes of the measured area of each section.

See also Video S1. The data were obtained by the Fourier transform ion cyclotron resonance (FT-ICR) mass spectrometer.

sections were then stained with hematoxylin and eosin and matched to a reference atlas. The monoamines were found to be highly abundant in the expected brain nuclei, thereby validating the specificity and spatial resolution of MSI (Figure 2A, Data S1). The dorsal raphe nucleus (DRN) and the median raphe nucleus (MRN) were extremely rich in 5-HT, the substantia nigra (SN) and the ventral tegmental area (VTA) had high DA levels, and an extremely high concentration of NE was observed in the locus coeruleus (LC) (Table 1). The concentration of DA in the striatum and nucleus accumbens, which are regions targeted by extensive dopaminergic innervation, was higher than that in the nuclei in which DA is produced (SN or VTA). Meanwhile, the concentration of 5-HT was highest in the DRN, which is the largest raphe nucleus

Brain Regions	5-HT	DA	NE
DRN	++++		++
SN	+++	++	
VTA	+++	++	
BLA/BMA	+++	++	
PVT	+++		++++
MRN	+++		
vPAG	++		+++
ReN/RhN	++		
cHip	++		
MiRN	++		
aBNST	+	+	
CP		+++++	
NAc		++++	
LC			++++
pBNST			++++
PHN			+++

Table 1. Major Brain Regions Enriched with Monoamines

DRN, dorsal raphe nucleus; SN, substantia nigra; VTA, ventral tegmental area; BLA/BMA, basolateral amygdala and basomedial amygdala; PVT, paraventricular nucleus of the thalamus; MRN, median raphe nucleus; vPAG, ventral part of the periaqueductal gray; ReN/RhN, reuniens nucleus and rhomboid nucleus; cHip, caudal part of the hippocampus; MiRN, midbrain raphe nucleus; aBNST, anterior division, anteromedial area, and anterior part of the bed nucleus of the stria terminalis; CP, caudate-putamen; NAc, nucleus accumbens; LC, locus coeruleus; pBNST, anterior division, anteromedial area, and posteroventral part of the bed nucleus of the stria terminalis; PHN, posterior hypothalamic nucleus.

(Table 1, Figure 2A). Such tendency in NE was not clearly elucidated. In addition, we detected other monoamine-rich nuclei. DA was abundant in the basolateral and basomedial amygdala (BLA/BMA) and 5-HT was rich in the SN, VTA, BLA/BMA, PVT, reuniens nucleus and rhomboid nucleus (ReN/RhN), caudal part of the hippocampus (cHip), and midbrain raphe nucleus (MiRN). NE was abundant in the PVT, posteroventral part of the bed nucleus of the stria terminalis (pBNST), ventral part of the periaqueductal gray (vPAG), posterior hypothalamic nucleus (PHN), and DRN (Table 1). To the best of our knowledge, the functions of 5-HT or NE in the PVT and ReN/RhN are not known (Cassel et al., 2013; Do Monte et al., 2016). Next, we generated tridimensional distributions of the three monoamines using a set of 15 coronal sections from another C57BL/6J male mouse of the same age. 5-HT, DA, and NE were widely distributed through the brain nuclei and forebrain, mainly with a non-overlapping pattern (Figure 2B and Video S1). The monoamine concentrations were high in the whole limbic system but significantly lower in the cortex, indicating their different qualitative roles in different regions. Moreover, monoamine neurotransmitters presented a non-overlapping distribution pattern, except in few regions, thereby indicating a mutually exclusive regulation in most brain nuclei.

Co-localization of 5-HT and Catecholamines

The simultaneous imaging of the three monoamines facilitated the identification of few areas of monoamine co-localization. We then focused our analysis on these regions. Monoamines modulate neuronal activity based on other neurotransmitters, and they can affect other functions (Hamon and Blier, 2013; Niederkofler et al., 2015; Pudovkina et al., 2002). For example, 5-HT acts on dopaminergic neurons in the SN, thereby suppressing the production of DA (Cobb and Abercrombie, 2003; Patel et al., 2004). Therefore, the presence of multiple monoamines in some regions of the brain indicates that they might be regulatory sites in which different monoaminergic systems directly interact. We detected the co-localization of 5-HT

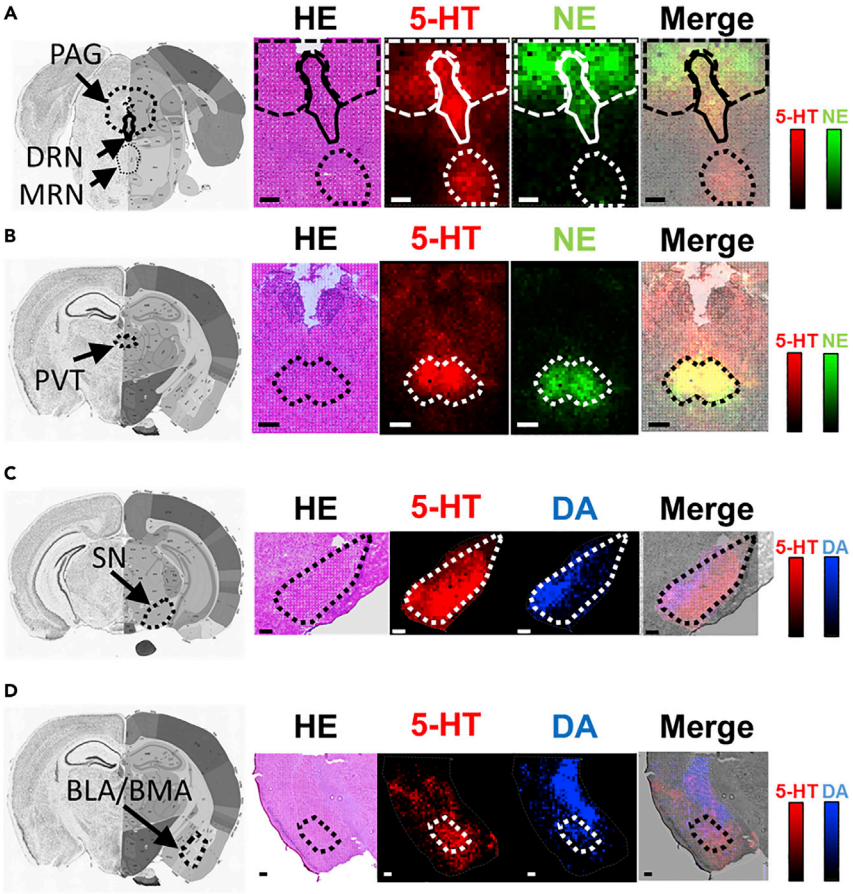

Figure 3. Representative Images Showing the Co-localization of 5-HT and Catecholamine in the Brain Nuclei

Reference coronal brain atlas, hematoxylin and eosin staining findings, graphical representation of 5-HT levels, catecholamine (NE or DA) levels, and merged 5-HT and catecholamine are shown from left to right.

(A) Ventral part of the periaqueductal gray (PAG) and dorsal raphe nucleus (DRN).

(B) Paraventricular nucleus of the thalamus (PVT).

(C and D) (C) Substantia nigra (SN) and (D) basolateral/basomedial amygdala (BLA/BMA). Scale bars, 200 μm. Data were obtained using the FT-ICR mass spectrometer.

and NE in the DRN, but not in the MRN, and in the vPAG, akin to the PVT (Figures 3A and 3B). 5-HT and DA were found in the SN (Figure 3C), BLA/BMA (Figure 3D), and VTA (Figure 2A, Supplemental Information). Thus, we identified multiple sites where 5-HT co-localized with either DA or NE. In contrast, none of the nuclei were rich in both NE and DA. These results indicated that 5-HT has a unique potential of integrating to the three monoaminergic signaling networks because it overlaps with the other two systems in several major brain nuclei, including the SN.

Quantitative Comparison Identifies PVT as a 5-HT-Rich Nucleus

Our study aimed to quantify the levels of 5-HT in several 5-HT-rich brain nuclei. We selected three coronal sections and mapped the concentration of 5-HT in six regions of interest: the DRN, SN, PVT, BLA/BMA, and hippocampus, divided in its caudal (cHip) and rostral parts (rHip) (Figure 4A). Among these regions, the somata of the serotonergic neurons can be found only in the DRN, where the highest concentration of 5-HT was observed. The average quantities of 5-HT in the SN and PVT were unexpectedly high, which were approximately 40% of the DRN value (Figure 4B). Therefore, the SN and PVT are the main brain regions targeted by serotonergic signaling in the steady state. The average quantities of 5-HT in the BLA/BMA, cHip, and rHip were 20%, 16%, and 10% of that detected in the DRN, respectively. Although minimal, the difference between cHip and rHip was statistically significant.

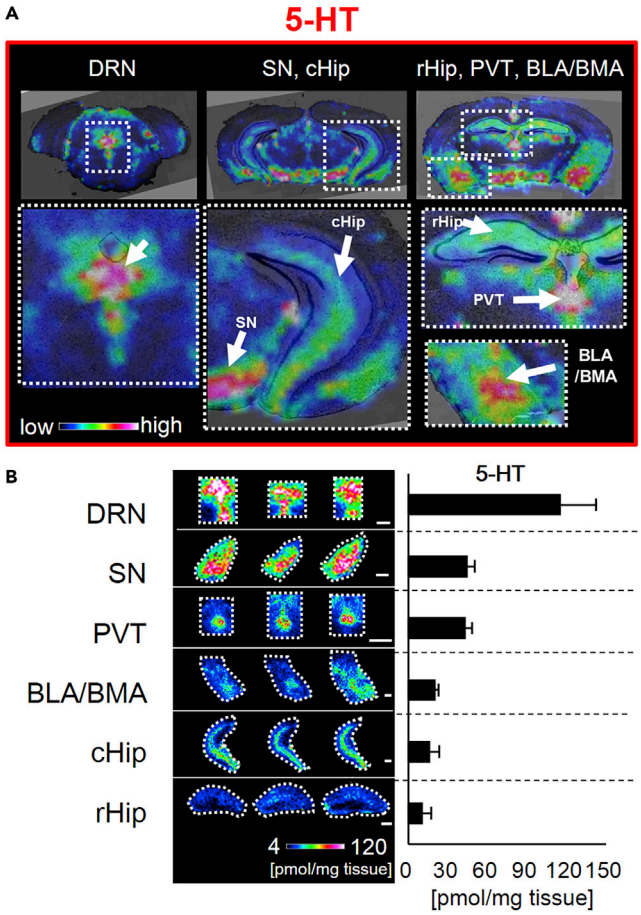

Figure 4. Quantitative Comparison of 5-HT in Selected Brain Nuclei

(A) Representative ion images showing the quantities of 5-HT-DPP in selected brain nuclei. The color scales were adjusted for each section. DRN, dorsal raphe nucleus; SN, substantia nigra; cHip, caudal part of the hippocampus; rHip, rostral part of the hippocampus; PVT, paraventricular nucleus of the thalamus; BLA/BMA, basolateral/basomedial amygdala.

(B) Left. Ion images showing 5-HT in the selected brain regions of three mice. Scale bar, 500 μm. The color scale depicting 5-HT quantitation is shown in the figure panel. Right. Averaged quantities of 5-HT per tissue weight in the regions shown in the panel. Data were presented as mean ± SD; mice, n = 3. Data were obtained using the FT-ICR mass spectrometer.

Classification of Brain Nuclei Based on Changes in 5-HT Level in the ATD Model

The serotonergic axon terminals targeting SN and PVT belong to different subsets of raphe neurons (Kiyasova et al., 2011; Muzerelle et al., 2016). Therefore, we hypothesized that the metabolic regulation of 5-HT differs among these nuclei. To test this possibility, we used the ATD model in which the mice received two oral administrations of a mixture of amino acids devoid of Trp (hereafter AAmix). A lower Trp level in the blood and brain was observed in the ATD model than in the water gavage group (Biskup et al., 2012) since essential amino acids in the Trp-free diet increases protein synthesis (Gessa et al., 1974; Moja et al., 1991) and large neutral amino acids compete with Trp in entering into the brain across the blood-brain barrier (Gessa et al., 1974). In addition, the decrease in Trp concentration in the blood affects anxiety-related behaviors (Biskup et al., 2012; Crockett et al., 2012; Young, 2013). Thus, ATD was expected to reduce the 5-HT levels in the brain nuclei, and Trp supplementation would increase them. To test this hypothesis, we used BALB/c mice, which have demonstrated decreased anxiety behavior on the ATD protocol (Biskup et al., 2012). MSI techniques were used to visualize the fluctuation of 5-HT in the SN and PVT after ATD. We then supplemented the mice with $^{13}C^{15}N$-labeled Trp ($^{13}C^{15}N$-Trp) to monitor the *de novo* synthesis of mass-labeled 5-HT ($^{13}C^{15}N$-5HT) (Figures 5A and 5B). The concentration of total Trp (the sum of Trp and $^{13}C^{15}N$-Trp) in the blood of mice receiving AAmix was lower by 70% than that of the control group receiving

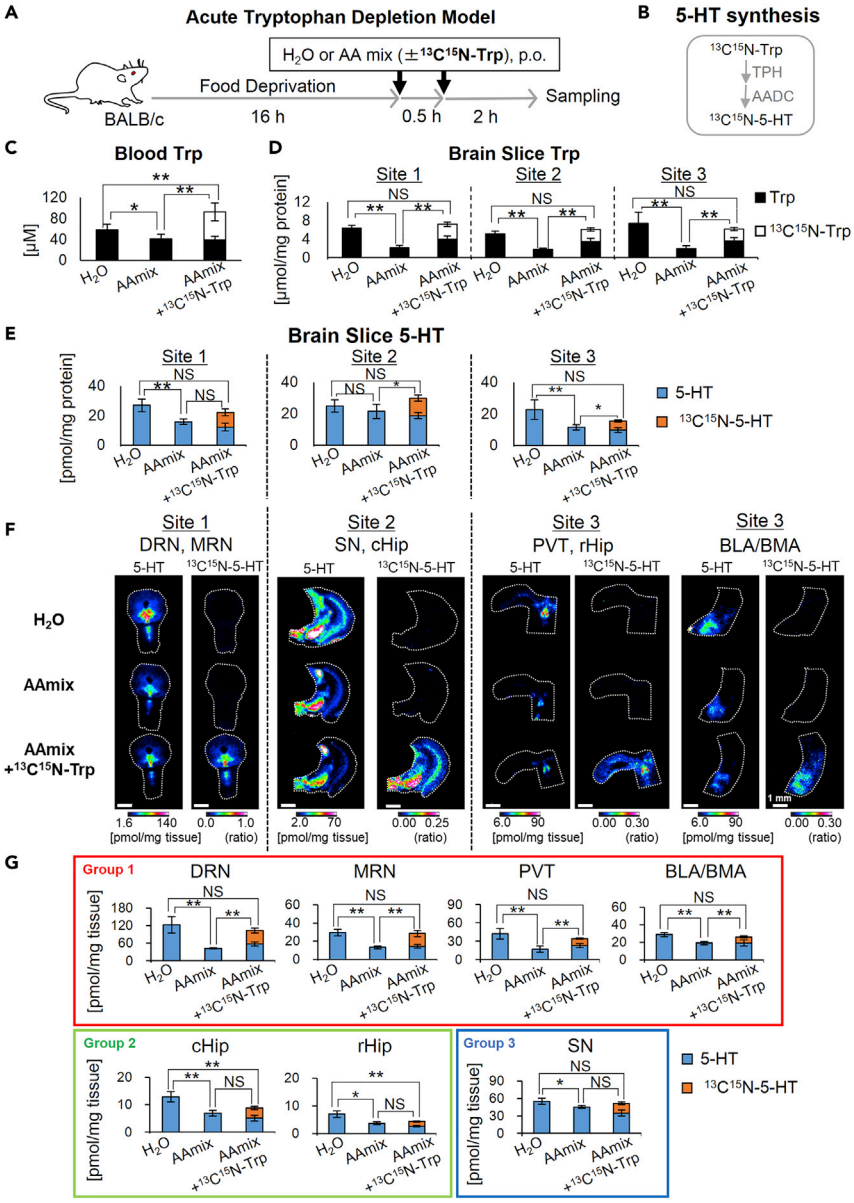

Figure 5. Classification of Brain Nuclei Based on 5-HT Turnover Using an ATD Model

(A) Schematics of the ATD experiment. After 16 h of food deprivation, the BALB/c mice were gavaged twice with H_2O, amino acid mixture without tryptophan (AAmix), or AAmix supplemented with labeled tryptophan (AAmix + $^{13}C^{15}N$-Trp) at an interval of 30 min.

(B) Synthetic pathway of $^{13}C^{15}N$-5-HT from $^{13}C^{15}N$-Trp. TPH, tryptophan hydroxylase; AADC, Aromatic L-amino acid decarboxylase.

(C) Concentration of tryptophan (Trp) and $^{13}C^{15}N$-Trp in the whole blood (mice gavaged with H_2O, AAmix, and AAmix + $^{13}C^{15}N$-Trp: n = 9, 11, and 10, respectively).

(D) Normalized amounts of Trp and $^{13}C^{15}N$-Trp in the extracts of whole brain slices at three sites (mice per group: n = 5, 5, and 5, respectively).

(E) Normalized amounts of 5-HT (blue) and labeled $^{13}C^{15}N$-5-HT (orange, synthesized from $^{13}C^{15}N$-Trp) in three whole coronal brain sections. Site 1 includes DRN and MRN; site 2 includes SN and cHip; site 3 includes PVT, rHip, and BLA/BMA (mice gavaged with H_2O, AAmix, and AAmix+$^{13}C^{15}N$-Trp: n = 5, 5, and 5, respectively).

(F) Representative ion images of 5-HT-DPP and $^{13}C^{15}N$-5-HT-DPP in the sections consecutive to the ones analyzed in (C). Note that the measured areas do not cover the whole sections.

Figure 5. *Continued*

(G) Classification of the seven nuclei based on 5-HT turnover. The bars show normalized amounts of 5-HT (blue) and labeled $^{13}C^{15}N$-5-HT (orange, synthetized from $^{13}C^{15}N$-Trp) in the indicated brain nuclei (mice for BLA/BMA, n = 4 and mice for other nuclei per group, n = 5).

Data in (C), (D), (E), and (G) were presented as mean ± SD. *, $p < 0.05$; **, $p < 0.005$ (Tukey's HSD test). DRN, dorsal raphe nucleus; MRN, median raphe nucleus; PVT, paraventricular nucleus of the thalamus; BLA/BMA, basolateral/basomedial amygdala; cHip, caudal part of the hippocampus; rHip, rostral part of the hippocampus; SN, substantia nigra. Data in (F) and (G) were obtained using the FT-ICR mass spectrometer.

water gavages, corresponding to 44% of the group receiving the AAmix with $^{13}C^{15}N$-Trp (Figure 5C). We evaluated the total amounts of Trp and 5-HT in the extracts of brain coronal slices at three sites: site 1, including DRN and MRN; site 2, including SN and rHip; and site 3, including PVT, cHip, and BLA/BMA. The ATD treatment substantially decreased the total concentration of Trp to 34%, 36%, and 27% of the control levels in sites 1, 2, and 3, respectively, and the co-administration of AAmix and $^{13}C^{15}N$-Trp restored the Trp levels to control levels (Figure 5D). Smaller variations in 5-HT levels were observed: the 5-HT levels significantly decreased to 59% and 51% in sites 1 and 3, respectively, compared with control levels, but not in site 2. The co-administration of AAmix and $^{13}C^{15}N$-Trp significantly increased the total 5-HT levels in sites 2 and 3, but not in site 1, compared with the administration of AAmix alone (Figure 5E).

We then analyzed the 5-HT metabolism in seven 5-HT-rich nuclei (DRN, MRN, SN, PVT, rHip, cHip, and BLA/BMA). We readily detected both unlabeled and newly synthesized 5-HT ($^{13}C^{15}N$-5HT) in all the nuclei (Figures 5F and S1). The 5-HT level in the PVT was significantly reduced by ATD (AAmix group versus water gavage group, Figure S2, left panel) and was increased with the supplementation of $^{13}C^{15}N$-Trp, a kinetic similar to DRN and MRN (Figure S2, right panel). We classified the seven nuclei into three groups based on their 5-HT metabolism (Figure 5G). In the first group, which included DRN, MRN, PVT, and BLA/BMA, the total 5-HT level decreased in response to ATD, but the levels increased to control level with the addition of $^{13}C^{15}N$-Trp to the AAmix (Figure 5G, red rectangle). In the second group, which comprised cHip and rHip, ATD led to a significant decrease in total 5-HT levels, but the levels did not increase with the addition of $^{13}C^{15}N$-Trp to the AAmix (Figure 5G, green rounded rectangle). In the third group, which consisted of SN alone, the total 5-HT level was only marginally affected by the depletion and repletion of Trp (Figure 5G, blue rounded rectangle). These findings showed that PVT belongs to a group of nuclei metabolically comparative with the DRN, MRN, and BLA/BMA, indicating that its function is modulated in a similar time frame and that it may play a similar role in regulating anxiety-like behavior. The metabolism of 5-HT differed between the hippocampus and SN, which is consistent with their limited relevance to anxiety-like behavior. We examined tryptophan hydroxylase 1 (TPH1)-deficient mice that cannot synthesize 5-HT in the peripheral tissues and pineal gland (Cote et al., 2003; Patel et al., 2004). In these mice, the pineal gland and the lumen of the blood vessels, but not DRN and PVT, showed a significant reduction in 5-HT levels (Figure S3). The result supports the concept that the function of PVT is modulated by serotonergic neurons that synthesize 5-HT in a TPH1-independent fashion via TPH2 (Mosienko et al., 2012; Patel et al., 2004).

To obtain more insights about the fate of 5-HT newly synthesized from labeled Trp in the blood, we compared the $^{13}C^{15}N$-5-HT levels over time in the DRN, MRN, PVT, rHip, and SN after the oral administration of AAmix plus $^{13}C^{15}N$-Trp (Figure S4A). In the DRN and MRN, $^{13}C^{15}N$-5-HT peaked at 45–90 min and then rapidly decreased. In other regions, the $^{13}C^{15}N$-5-HT levels remained relatively low and reached their maximum levels at 150–300 min (Figure S4B). In addition, the $^{13}C^{15}N$-5-HT level in the rHip was lower than that in the PVT and SN during the entire experimental time course (600 min) (Figure S4B).

In the ATD experimental setting, the synthesis of 5-HT in the brain depends on both the rate of Trp import across the blood-brain barrier and the rate of its enzymatic conversion into 5-HT. To provide a more direct evidence, we administrated $^{13}C^{15}N$-Trp into the DRN and MRN (Figure 6A). Two and a half hours later, most 5-HT in the DRN and MRN were newly synthesized as $^{13}C^{15}N$-5-HT (Figure 6B). At the same time point, we detected high levels of $^{13}C^{15}N$-5-HT in the PVT and SN but not in the rHip (Figures 6B, 6C, and S5). These results showed that the serotonergic neurons in the DRN and MRN prioritize the delivery of 5-HT to the PVT and SN rather than the rHip.

DISCUSSION

Herein, we report a new mouse whole brain atlas of 5-HT, DA, and NE using MSI. Our data represent an entire map of physiological monoamine level in the mouse brain, thereby opening the venue to more

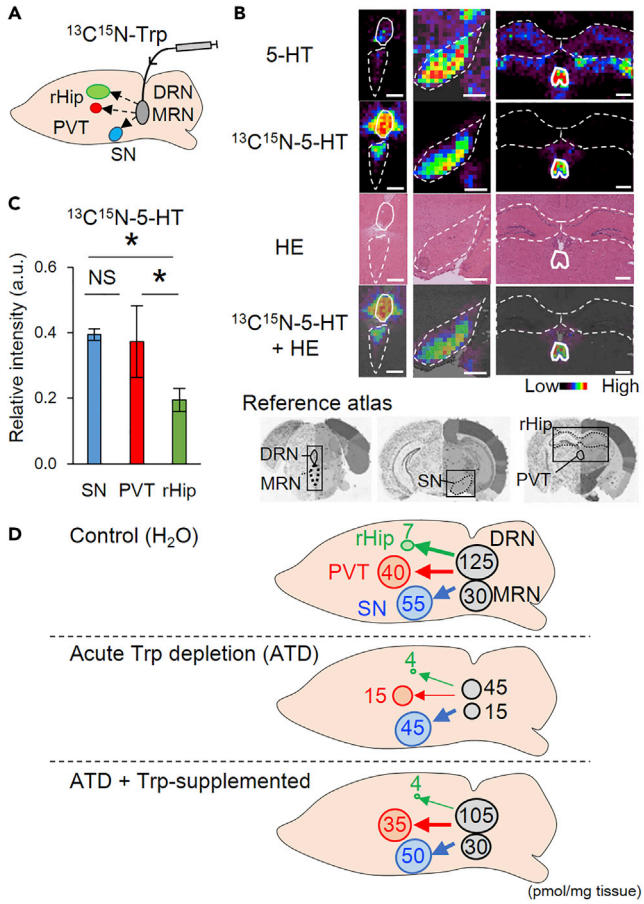

Figure 6. Distribution of the Newly Synthesized 5-HT Provided from the DRN and MRN

(A) Schematic diagram of the experimental procedure. Continuous infusion of $^{13}C^{15}N$-Trp to the DRN and MRN lasted for 2.5 h.

(B) From the top line. Levels of 5-HT and $^{13}C^{15}N$-5-HT, H&E staining of the same sections performed after measurement, and merged images of the $^{13}C^{15}N$-5-HT and the H&E stain. The reference coronal brain atlas is shown at the bottom. Scale bar, 500 μm.

(C) Comparison of the relative abundance of $^{13}C^{15}N$-5-HT between the indicated regions. SN, substantia nigra; PVT, paraventricular nucleus of the thalamus; rHip, rostral hippocampus. Data were presented as mean ± SD (n = 3 mice), *, $p < 0.05$ (Tukey's HSD test).

(D) A model of the pathway-specific adjustment of 5-HT delivery. The arrows show the levels of newly synthetized 5-HT irradiating along the serotonergic neurons from the DRN and MRN. Thick arrows represent a preferential supply, and thin arrows low priority supply. The size of the circle at each nucleus showed the level of pooled 5HT based on Figure 3G. The relative distribution in the control, ATD model, and Trp-supplemented groups are shown in the top, center, and bottom, respectively. Data were obtained using the linear ion trap mass spectrometer.

precise studies of their functions. Currently, most data about monoamine distributions in the brain are based on the gene expression of the key neuronal synthetic enzymes (Nagatsu, 1991; Patel et al., 2004): TPH for 5-HT, tyrosine hydroxylase for DA, and dopamine beta hydroxylase for NE. Even if a direct correlation exists between metabolic key enzymes and the production of their respective monoamines, we must consider that the availability of monoamines in the brain is affected by the catabolic activity of monoamine oxidases A and B (Shih et al., 1999) or catechol-O-methyltransferase (Gogos et al., 1998) and even further by the reuptake transporters (Bermingham and Blakely, 2016) recycling the secreted monoamines from extracellular sites.

Direct mapping of the brain monoamine levels was extremely challenging since it requires both quantitative detection and spatial resolution: the two analytical requisites are generally fulfilled using different

techniques. The best quantitative performance is currently guaranteed by a chromatograph equipped with a detector (e.g., liquid chromatograph-electrochemical detector and gas chromatograph-mass spectrometer [Aragon et al., 2017; Miyajima et al., 2017]). Such instruments can be combined to sampling techniques, such as laser microdissection, to map quantities of a target molecule (Franck et al., 2013). However, these approaches are highly time consuming and are not suitable for high-throughput analyses. Alternatively, histochemical fluorescence-based imaging techniques, such as the Falck-Hillarp method (Falck and Hillarp, 1959) and IHC as well as ARG, have been used to identify the presence of monoamine nuclei in the brain (Fuxe et al., 2007; Masuoka and Alcaraz, 1975). The discovery of the monoaminergic neurons was achieved using the Falck-Hillarp method (Carlsson et al., 1962; Falck and Hillarp, 1959; Falck and Torp, 1962) by which fluorescence signals from derivatives of monoamines can be observed under a microscope. The method was the first useful method for histochemical monoamines analysis; however, its specificity and precision were not sufficient to perform a quantitative comparison or monitoring of monoamine levels. IHC for conjugated (immunoreactive) monoamines was developed at a later time, and most data about monoaminergic pathways are based on IHC data. However, IHC is affected by intrinsic variability and is not robust enough to compare large sets of samples (Nielsen et al., 2006). Our atlas showed a more physiological distribution of the monoamines than the previously reported ones (Steinbusch, 1981) since no drugs were administered before brain imaging and the samples were neither perfused nor fixed. ARG, which includes positron emission tomography, conjugates high spatial resolution, sensitivity, and quantitative performance (Masuoka and Alcaraz, 1975; Takano, 2018). However, despite being useful to chase injected molecules, it cannot detect unmodified brain monoamines.

Our data showed that monoamine quantities vary between the cell bodies and axon terminals, thereby possibly reflecting the different rates of synthesis or transport within single neurons. Indeed, previous studies have shown the different metabolic activities in the nuclei innervated by the monoaminergic axons supporting the former view (Halaris et al., 1976; Kim et al., 2005). It should be considered that the secreted monoamines either mediate synaptic transmission or diffuse in the extracellular space and bind to distant, extrasynaptic receptors on multiple target neurons. The latter type of transmission, referred to as volume transmission (Fuxe et al., 2010), involves a significant proportion of the axon terminals of monoaminergic neurons and helps to control various brain functions, despite their small number. MSI likely detects monoamines belonging to both pools. However, it cannot discriminate between intracellular compartments (i.e., soma, dendrites, and axons) and intracellular/extracellular monoamines, since the minimum spatial resolution for the monoamines is about 1–3 μm (Kaya et al., 2018; Kompauer et al., 2016; Passarelli et al., 2017). Although a higher spatial resolution <1 μm may be achieved using secondary ion mass spectrometry in the near future (Kaya et al., 2018; Passarelli et al., 2017), the use of MSI combined with other techniques that detect extracellular monoamines (i.e., microdialysis [Chen et al., 1999], fast-scan cyclic voltammetry [Borue et al., 2010]) as well as optogenetics (Takata et al., 2018; Watanabe et al., 2018) or fiber photometry (Tsutsui-Kimura et al., 2017) is essential to better understand the monoaminergic regulation of animal behaviors. We anticipate that further MSI analysis of monoamine turnover will provide direct evidence of synthesis, transport, and regional availability of the brain monoamines.

In the course of this study, we identified several brain nuclei in which high concentrations of 5-HT and one catecholamine overlapped, indicating that they are nodes of reciprocal regulation between different monoaminergic networks. Indeed, several reports have shown the functional interaction of multiple monoamines in some nuclei (e.g., 5-HT and NE at the DRN [Baraban and Aghajanian, 1980; Pudovkina et al., 2002], 5-HT and DA at the SN [Burke et al., 2014; Cobb and Abercrombie, 2003; Demireva et al., 2018; Lindgren et al., 2010], and 5-HT and DA at the VTA [Alex and Pehek, 2007; Prisco et al., 1994]). The sites of DA production (the SN and VTA) showed high 5-HT levels, thereby indicating that the dopaminergic system may be controlled by 5-HT (Doly et al., 2017; Niederkofler et al., 2015). Similarly, the central site of 5-HT production, which is the DRN, showed a high NE level, indicating a similar relationship. By contrast, in the site of NE production, the level of other monoamines was not high in the LC. Therefore, LC may play a central role in monoaminergic regulation (Figure S6). We do not exclude the possibility that neurotransmitters, other than 5-HT or DA, regulate noradrenergic neurons in the LC, in analogy with a proposed model in the rat brain (Aston-Jones, 2004).

We performed the metabolic characterization of 5-HT-rich nuclei manipulating the levels of Trp in the blood, a procedure known to affect both the 5-HT synthesis in the brain and anxiety-like behavior in the

BALB/c mice. We note that C57BL/6J mice commonly show reductions of Trp and 5-HT levels after the ATD treatment, although their behavior was unchanged (Biskup et al., 2012). Such differences are likely due to more serotonergic (TPH2 positive) neurons and higher 5-HT content of C57BL/6J mice when compared with BALB/c mice (Bach et al., 2011).

We identified two brain nuclei (BLA/BMA and PVT) with 5-HT kinetics similar to the major raphe nuclei (DRN and MRN). In these nuclei, the 5-HT concentrations closely followed the availability of Trp in the blood, rapidly decreasing after the depletion of Trp, and were rescued by newly synthetized 5-HT during the administration of Trp. Therefore, they may be correlated to anxiety-like behavior associated with ATD. Indeed, the 5-HT levels in the BLA/BMA, DRN, and MRN regulate anxiety-like behavior (Johnson et al., 2015; Marcinkiewcz et al., 2016; Teissier et al., 2015). Notably, PVT neurons project into the amygdala, and the inhibition of PVT causes abnormal fear responses (Do-Monte et al., 2015; Kirouac, 2015; Do Monte et al., 2016; Penzo et al., 2015) and depressive-like behavior (Kasahara et al., 2016). However, as these studies are based on PVT inhibition or deletion, they do not provide information about the effect of 5-HT in PVT on behavior (Pratelli et al., 2017; Steinbusch, 1981; Vertes et al., 2010). The findings of the present study indicate that 5-HT in PVT may play an important role in the control of anxiety-like behavior, which may have been substantially overlooked. We anticipate that the 5-HT_7 receptor could be involved because of its highly localized expression in the PVT (Neumaier et al., 2001).

We revealed that newly synthesized 5-HT is rapidly conveyed from the raphe nuclei to the PVT and SN, rather than to the rHip. We considered that the delivery to the PVT, SN, and rHip could be summarized, as depicted in Figure 6D. If the levels of peripheral Trp are not limiting, 5-HT neurons in the DRN and MRN convert Trp to 5-HT and provide the new 5-HT preferentially to the PVT and SN rather than rHip. When the levels of peripheral Trp decrease, as in the ATD model or in our previous model of chronic immune activation (Miyajima et al., 2017), the delivery of 5-HT to PVT and rHip significantly decreases, whereas that to the SN is less affected. Supplementation with Trp restored the supply of 5-HT to the PVT and SN but not to the rHip. Our results support the idea that the serotonergic nervous system targets different brain regions with different priorities. This finding could facilitate a better understanding of the complexity of the serotonergic network in the brain.

Limitations of the Study

In this study, the whole brain atlas of 5-HT, DA, and NE was built using an animal (8-week-old C57BL/6J male mouse) as a preceding model. We confirmed consistency and reproducibility regarding high levels of 5-HT in DRN, MRN, SN, PVT, rHip, cHip, and BLA/BMA. However, further studies examining other strains at different ages are required to establish a generalized atlas.

Despite the fact that MSI can be used to identify specific brain nuclei in which monoamines are dynamically fluctuated, it cannot distinguish changes in extracellular spaces from those in the intracellular fraction. By using other techniques to monitor released monoamine concentrations, such as microdialysis or fast-scan cyclic voltammetry, complementary information that is essential for understanding how the alteration in monoamine metabolism affects animal behavior can be obtained.

METHODS

All methods can be found in the accompanying Transparent Methods supplemental file.

SUPPLEMENTAL INFORMATION

Supplemental Information can be found online at https://doi.org/10.1016/j.isci.2019.09.036.

ACKNOWLEDGMENTS

This work was supported by JSPS KAKENHI under grant number 16H06145 (to Y.S.); AMED under grant numbers JP18gm0710012 (to S.F. and Y.S.), JP18dm030727 (to Y.S. and E.S.), and JP18gm0910004 (to M.S.); AMED–CREST under grant number 14532135 (to S.F.); the Takeda Science Foundation (to E.S.); the Swedish Research Council (Medicine and Health no. 2018–03320, Natural and Engineering Science no. 2018–05501); the Swedish Brain Foundation; the Swedish Foundation for Strategic (no. RIF14-0078); and Science for Life Laboratory (SciLifeLab) (to P.E.A).

AUTHOR CONTRIBUTIONS

Y.S. conceived the conceptual design of the study. E.S., S.F., Ma.S., K.F.T., Mi.S., and P.E.A. contributed to the conceptual design. E.S., M.M.G., K.H., Y.H., M.A., and K.F.T. performed the experiments. E.S., M.M.G., Y.H., and P.K. analyzed the results. E.S. and Y.S. wrote the manuscript. M.M.G., S.F., Ma.S., K.F.T., and P.E.A. contributed in the writing and revision of the manuscript.

DECLARATION OF INTERESTS

The authors declare no competing interests.

Received: December 27, 2018
Revised: July 12, 2019
Accepted: September 24, 2019
Published: October 25, 2019

REFERENCES

Alex, K.D., and Pehek, E.A. (2007). Pharmacologic mechanisms of serotonergic regulation of dopamine neurotransmission. Pharmacol. Ther. *113*, 296–320.

Aragon, A., Legradi, J., Ballesteros-Gómez, A., Legler, J., van Velzen, M., de Boer, J., and Leonards, P. (2017). Determination of monoamine neurotransmitters in zebrafish (*Danio rerio*) by gas chromatography coupled to mass spectrometry with a two-step derivatization. Anal. Bioanal. Chem. *409*, 2931–2939.

Aston-Jones, G. (2004). Locus Coeruleus, A5 and A7 Noradrenergic Cell Groups. In The Rat Nervous System, G. Paxino, ed. (Academic Press), pp. 259–294.

Aston-Jones, G., and Cohen, J.D. (2005). An integrative theory of locus coeruleus-norepinephrine function: adaptive gain and optimal performance. Annu. Rev. Neurosci. *28*, 403–450.

Bach, H., Arango, V., Huang, Y.Y., Leong, S., John Mann, J., and Underwood, M.D. (2011). Neuronal tryptophan hydroxylase expression in BALB/cJ and C57Bl/6J mice. J. Neurochem. *118*, 1067–1074.

Baraban, J.M., and Aghajanian, G.K. (1980). Suppression of firing activity of 5-HT neurons in the dorsal raphe by alpha-adrenoceptor antagonists. Neuropharmacology *19*, 355–363.

Benazzouz, A., Mamad, O., Abedi, P., Bouali-Benazzouz, R., and Chetrit, J. (2014). Involvement of dopamine loss in extrastriatal basal ganglia nuclei in the pathophysiology of Parkinson's disease. Front. Aging Neurosci. *6*, 1–5.

Bermingham, D.P., and Blakely, R.D. (2016). Kinase-dependent regulation of monoamine neurotransmitter transporters. Pharmacol. Rev. *68*, 888–953.

Biskup, C.S., Sánchez, C.L., Arrant, A., van Swearingen, A.E.D., Kuhn, C., and Zepf, F.D. (2012). Effects of acute tryptophan depletion on brain serotonin function and concentrations of dopamine and norepinephrine in C57BL/6J and BALB/cJ mice. PLoS One *7*, 7–14.

Borue, X., Condron, B., and Venton, B.J. (2010). Both synthesis and reuptake are critical for replenishing the releasable serotonin pool in Drosophila. J. Neurochem. *113*, 188–199.

Burke, M.V., Nocjar, C., Sonneborn, A.J., McCreary, A.C., and Pehek, E.A. (2014). Striatal serotonin 2C receptors decrease nigrostriatal dopamine release by increasing GABA-A receptor tone in the substantia nigra. J. Neurochem. *131*, 432–443.

Caprioli, R.M., Farmer, T.B., and Gile, J. (1997). Molecular imaging of biological samples: localization of peptides and proteins using MALDI-TOF MS. Anal. Chem. *69*, 4751–4760.

Carlsson, A., Falck, B., and Hillarp, N.Å. (1962). Cellular localization of brain monoamines. Acta Physiol. Scand. Suppl. *56*, 1–28.

Cassel, J.C., Pereira de Vasconcelos, A., Loureiro, M., Cholvin, T., Dalrymple-Alford, J.C., and Vertes, R.P. (2013). The reuniens and rhomboid nuclei: neuroanatomy, electrophysiological characteristics and behavioral impsupplications. Prog. Neurobiol. *111*, 34–52.

Chen, L., He, M., Sibille, E., Thompson, A., Sarnyai, Z., Baker, H., Shippenberg, T., and Toth, M. (1999). Adaptive changes in postsynaptic dopamine receptors despite unaltered dopamine dynamics in mice lacking monoamine oxidase B. J. Neurochem. *73*, 647–655.

Cobb, W.S., and Abercrombie, E.D. (2003). Differential regulation of somatodendritic and nerve terminal dopamine release by serotonergic innervation of substantia nigra. J. Neurochem. *84*, 576–584.

Cote, F., Thevenot, E., Fligny, C., Fromes, Y., Darmon, M., Ripoche, M.-A., Bayard, E., Hanoun, N., Saurini, F., Lechat, P., et al. (2003). Disruption of the nonneuronal tph1 gene demonstrates the importance of peripheral serotonin in cardiac function. Proc. Natl. Acad. Sci. U S A *100*, 13525–13530.

Crockett, M.J., Clark, L., Roiser, J.P., Robinson, O.J., Cools, R., Chase, H.W., den Ouden, H., Apergis-Schoute, A., Campbell-Meiklejohn, D., Campbell-Meikeljohn, D., et al. (2012). Converging evidence for central 5-HT effects in acute tryptophan depletion. Mol. Psychiatry *17*, 121–123.

Do-Monte, F.H., Quinõnes-Laracuente, K., and Quirk, G.J. (2015). A temporal shift in the circuits mediating retrieval of fear memory. Nature *519*, 460–463.

Doly, S., Quentin, E., Eddine, R., Tolu, S., Fernandez, S.P., Bertran-Gonzalez, J., Valjent, E., Belmer, A., Viñals, X., Callebert, J., et al. (2017). Serotonin 2B receptors in mesoaccumbens dopamine pathway regulate cocaine responses. J. Neurosci. *37*, 1354–1417.

Esteve, C., Tolner, E.A., Shyti, R., van den Maagdenberg, A.M.J.M., and McDonnell, L.A. (2016). Mass spectrometry imaging of amino neurotransmitters: a comparison of derivatization methods and application in mouse brain tissue. Metabolomics *12*, 1–9.

Falck, B., and Hillarp, N.Å. (1959). On the cellular localization of catechol amines in the brain. Acta Anat (Basel) *38*, 277–279.

Falck, B., and Torp, A. (1962). New evidence for the localization of noradrenalin in the adrenergic nerve terminals. Med. Exp. *6*, 169–172.

Franck, J., Quanico, J., Wisztorski, M., Day, R., Salzet, M., and Fournier, I. (2013). Quantification-based mass spectrometry imaging of proteins by parafilm assisted microdissection. Anal. Chem. *85*, 8127–8134.

Fuxe, K., Dahlström, A., Höistad, M., Marcellino, D., Jansson, A., Rivera, A., Diaz-Cabiale, Z., Jacobsen, K., Tinner-Staines, B., Hagman, B., et al. (2007). From the Golgi-Cajal mapping to the transmitter-based characterization of the neuronal networks leading to two modes of brain communication: wiring and volume transmission. Brain Res. Rev. *55*, 17–54.

Fuxe, K., Dahlström, A.B., Jonsson, G., Marcellino, D., Guescini, M., Dam, M., Manger, P., and Agnati, L. (2010). The discovery of central monoamine neurons gave volume transmission to the wired brain. Prog. Neurobiol. *90*, 82–100.

Gantz, S.C., Levitt, E.S., Llamosas, N., Neve, K.A., and Williams, J.T. (2015). Depression of serotonin synaptic transmission by the dopamine Precursor L-DOPA. Cell Rep. *12*, 944–954.

Gessa, G.L., Biggio, G., Fadda, F., Corsini, G.U., and Tagliamonte, A. (1974). Effect of the oral administration of tryptophan-free amino acid

mixtures on serum tryptophan, brain tryptophan and serotonin metabolism. J. Neurochem. *22*, 869–870.

Gogos, J.A., Morgan, M., Luine, V., Santha, M., Ogawa, S., Pfaff, D., and Karayiorgou, M. (1998). Catechol-O-methyltransferase-deficient mice exhibit sexually dimorphic changes in catecholamine levels and behavior. Proc. Natl. Acad. Sci. U S A *95*, 9991–9996.

Halaris, A.E., Jones, B.E., and Moore, R.Y. (1976). Axonal transport in serotonin neurons of the midbrain raphe. Brain Res. *107*, 555–574.

Hamon, M., and Blier, P. (2013). Monoamine neurocircuitry in depression and strategies for new treatments. Prog. Neuropsychopharmacol. Biol. Psychiatry *45*, 54–63.

Hardebo, J.E., and Owman, C. (1980). Barrier mechanisms for neurotransmitter monoamines and their precursors at the blood-brain interface. Ann. Neural. *8*, 1–11.

Johnson, P.L., Molosh, A., Fitz, S.D., Arendt, D., Deehan, G.A., Federici, L.M., Bernabe, C., Engleman, E.A., Rodd, Z.A., Lowry, C.A., et al. (2015). Pharmacological depletion of serotonin in the basolateral amygdala complex reduces anxiety and disrupts fear conditioning. Pharmacol. Biochem. Behav. *138*, 174–179.

Kasahara, T., Takata, A., Kato, T.M., Kubota-Sakashita, M., Sawada, T., Kakita, A., Mizukami, H., Kaneda, D., Ozawa, K., and Kato, T. (2016). Depression-like episodes in mice harboring mtDNA deletions in paraventricular thalamus. Mol. Psychiatry *21*, 39–48.

Kaya, I., Brülls, S.M., Dunevall, J., Jennische, E., Lange, S., Martensson, J., Ewing, A.G., Malmberg, P., and Fletcher, J.S. (2018). On-tissue chemical derivatization of catecholamines using 4-(N-Methyl)pyridinium boronic acid for ToF-SIMS and LDI-ToF mass spectrometry imaging. Anal. Chem. *90*, 13580–13590.

Kim, D.K., Tolliver, T.J., Huang, S.J., Martin, B.J., Andrews, A.M., Wichems, C., Holmes, A., Lesch, K.P., and Murphy, D.L. (2005). Altered serotonin synthesis, turnover and dynamic regulation in multiple brain regions of mice lacking the serotonin transporter. Neuropharmacology *49*, 798–810.

Kirouac, G.J. (2015). Placing the paraventricular nucleus of the thalamus within the brain circuits that control behavior. Neurosci. Biobehav. Rev. *56*, 315–329.

Kiyasova, V., Fernandez, S.P., Laine, J., Stankovski, L., Muzerelle, A., Doly, S., and Gaspar, P. (2011). A genetically defined morphologically and functionally unique subset of 5-HT neurons in the mouse raphe nuclei. J. Neurosci. *31*, 2756–2768.

Kompauer, M., Heiles, S., and Spengler, B. (2016). Atmospheric pressure MALDI mass spectrometry imaging of tissues and cells at 1.4-μm lateral resolution. Nat. Methods *14*, 90–96.

Lindgren, H.S., Andersson, D.R., Lagerkvist, S., Nissbrandt, H., and Cenci, M.A. (2010). L-DOPA-induced dopamine efflux in the striatum and the substantia nigra in a rat model of Parkinson's disease: temporal and quantitative relationship to the expression of dyskinesia. J. Neurochem. *112*, 1465–1476.

Lucki, I. (1998). The spectrum of behaviors influenced by serotonin. Biol. Psychiatry *44*, 151–162.

Marcinkiewcz, C.A., Mazzone, C.M., D'Agostino, G., Halladay, L.R., Hardaway, J.A., Diberto, J.F., Navarro, M., Burnham, N., Cristiano, C., Dorrier, C.E., et al. (2016). Serotonin engages an anxiety and fear-promoting circuit in the extended amygdala. Nature *537*, 97–101.

Masuoka, D.T., and Alcaraz, A.F. (1975). An autoradiographic method of mapping the distribution and density of monoamine neurons in mouse brain. Eur. J. Pharmacol. *33*, 125–130.

McCall, J.G., Siuda, E.R., Bhatti, D.L., Lawson, L.A., McElligott, Z.A., Stuber, G.D., and Bruchas, M.R. (2017). Locus coeruleus to basolateral amygdala noradrenergic projections promote anxiety-like behavior. Elife *6*, 1–23.

Migliarini, S., Pacini, G., Pelosi, B., Lunardi, G., and Pasqualetti, M. (2013). Lack of brain serotonin affects postnatal development and serotonergic neuronal circuitry formation. Mol. Psychiatry *18*, 1106–1118.

Miyajima, M., Zhang, B., Sugiura, Y., Sonomura, K., Guerrini, M.M., Tsutsui, Y., Maruya, M., Vogelzang, A., Chamoto, K., Honda, K., et al. (2017). Metabolic shift induced by systemic activation of T cells in PD-1-deficient mice perturbs brain monoamines and emotional behavior. Nat. Immunol. *18*, 1342–1352.

Moja, E.A., Restani, P., Corsini, E., Stacchezzini, M.C., Assereto, R., and Galli, C.L. (1991). Cycloheximide blocks the fall of plasma and tissue tryptophan levels after tryptophan-free amino acid mixtures. Life Sci. *49*, 1121–1128.

Demireva, E.Y., Suri, D., Morelli, E., Mahadevia, D., Chuhma, N., Teixeira, C.M., Ziolkowski, A., Hersh, M., Fifer, J., Bagchi, S., et al. (2018). 5–HT2C receptor blockade reverses SSRI-associated basal ganglia dysfunction and potentiates therapeutic efficacy. Mol. Psychiatry In press.

Do Monte, F.H., Quirk, G.J., Li, B., and Penzo, M.A. (2016). Retrieving fear memories, as time goes by…. Mol. Psychiatry *21*, 1027–1036.

Mosienko, V., Bert, B., Beis, D., Matthes, S., Fink, H., Bader, M., and Alenina, N. (2012). Exaggerated aggression and decreased anxiety in mice deficient in brain serotonin. Transl. Psychiatry *2*, e122–e129.

Muzerelle, A., Scotto-Lomassese, S., Bernard, J.F., Soiza-Reilly, M., and Gaspar, P. (2016). Conditional anterograde tracing reveals distinct targeting of individual serotonin cell groups (B5–B9) to the forebrain and brainstem. Brain Struct. Funct. *221*, 535–561.

Nagatsu, T. (1991). Genes for human catecholamine-synthesizing enzymes. Neurosci. Res. *12*, 315–345.

Neumaier, J.F., Sexton, T.J., Yracheta, J., Diaz, A., and Brownfield, M. (2001). Localization of 5-HT 7 receptors in rat brain by immunocytochemistry, in situ hybridization, and agonist stimulated cFos expression. J. Chem. Neuroanat. *21*, 63–73.

Niederkofler, V., Asher, T.E., and Dymecki, S.M. (2015). Functional interplay between dopaminergic and serotonergic neuronal systems during development and adulthood. ACS Chem. Neurosci. *6*, 1055–1070.

Nielsen, K., Brask, D., Knudsen, G.M., and Aznar, S. (2006). Immunodetection of the serotonin transporter protein is a more valid marker for serotonergic fibers than serotonin. Synapse *59*, 270–276.

Nilsson, A., Goodwin, R.J.A., Shariatgorji, M., Vallianatou, T., Webborn, P.J.H., and Andrén, P.E. (2015). Mass spectrometry imaging in drug development. Anal. Chem. *87*, 1437–1455.

Panigrahi, B., Martin, K.A., Li, Y., Mensh, B.D., Karpova, A.Y., Dudman, J.T., Panigrahi, B., Martin, K.A., Li, Y., Graves, A.R., et al. (2015). Dopamine is required for the neural representation and control of movement vigor article dopamine is required for the neural representation and control of movement vigor. Cell *162*, 1418–1430.

Passarelli, M.K., Pirkl, A., Moellers, R., Grinfeld, D., Kollmer, F., Havelund, R., Newman, C.F., Marshall, P.S., Arlinghaus, H., Alexander, M.R., et al. (2017). The 3D OrbiSIMS—label-free metabolic imaging with subcellular lateral resolution and high mass-resolving power. Nat. Methods *14*, 1175–1183.

Patel, P.D., Pontrello, C., and Burke, S. (2004). Robust and tissue-specific expression of TPH2 versus TPH1 in rat raphe and pineal gland. Biol. Psychiatry *55*, 428–433.

Penzo, M.A., Robert, V., Tucciarone, J., De Bundel, D., Wang, M., Van Aelst, L., Darvas, M., Parada, L.F., Palmiter, R.D., He, M., et al. (2015). The paraventricular thalamus controls a central amygdala fear circuit. Nature *519*, 455–459.

Pratelli, M., Migliarini, S., Pelosi, B., Napolitano, F., Usiello, A., and Pasqualetti, M. (2017). Perturbation of serotonin homeostasis during adulthood affects serotonergic neuronal circuitry. eNeuro *4*, 1–13.

Prisco, S., Pagannone, S., and Esposito, E. (1994). Serotonin-dopamine interaction in the rat ventral tegmental area: an electrophysiological study in vivo. J. Pharmacol. Exp. Ther. *271*, 83–90.

Pudovkina, O.L., Cremers, T.I.F.H., and Westerink, B.H.C. (2002). The interaction between the locus coeruleus and dorsal raphe nucleus studied with dual-probe microdialysis. Eur. J. Pharmacol. *445*, 37–42.

Schweighofer, N., Bertin, M., Shishida, K., Okamoto, Y., Tanaka, S.C., Yamawaki, S., and Doya, K. (2008). Low-serotonin levels increase delayed reward discounting in humans. J. Neurosci. *28*, 4528–4532.

Shariatgorji, M., Nilsson, A., Goodwin, R.J.A., Källback, P., Schintu, N., Zhang, X., Crossman, A.R., Bezard, E., Svenningsson, P., and Andren, P.E. (2014). Direct targeted quantitative molecular imaging of neurotransmitters in brain tissue sections. Neuron *84*, 697–707.

Shariatgorji, M., Nilsson, A., Källback, P., Karlsson, O., Zhang, X., Svenningsson, P., and Andren, P.E. (2015). Pyrylium salts as reactive matrices for MALDI-MS imaging of biologically

active primary amines. J. Am. Soc. Mass Spectrom. *26*, 934–939.

Shih, J.C., Chen, K., and Ridd, M.J. (1999). Monoamine oxidase: from genes to behavior. Annu. Rev. Neurosci. *22*, 197–217.

Singh, C., Oikonomou, G., and Prober, D.A. (2015). Norepinephrine is required to promote wakefulness and for hypocretin-induced arousal in zebrafish. Elife *4*, 1–22.

Steinbusch, H.W.M. (1981). Distribution of serotonin-immunoreactivity in the central nervous system of the rat-Cell bodies and terminals. Neuroscience *6*, 557–618.

Sugiura, Y., Zaima, N., Setou, M., Ito, S., and Yao, I. (2012). Visualization of acetylcholine distribution in central nervous system tissue sections by tandem imaging mass spectrometry. Anal. Bioanal. Chem. *403*, 1851–1861.

Sugiyama, E., Kondo, T., Kuzumaki, N., Honda, K., Yamanaka, A., Narita, M., Suematsu, M., and Sugiura, Y. (2019). Mechanical allodynia induced by optogenetic sensory nerve excitation activates dopamine signaling and metabolism in medial nucleus accumbens. Neurochem. Int. *129*, 104494.

Takano, H. (2018). Cognitive function and monoamine neurotransmission in Schizophrenia: evidence from positron emission tomography studies. Front. Psychiatry *9*, 1–8.

Takata, N., Sugiura, Y., Yoshida, K., Koizumi, M., Hiroshi, N., Honda, K., Yano, R., Komaki, Y., Matsui, K., Suematsu, M., et al. (2018). Optogenetic astrocyte activation evokes BOLD fMRI response with oxygen consumption without neuronal activity modulation. Glia *66*, 2013–2023.

Teissier, A., Chemiakine, A., Inbar, B., Bagchi, S., Ray, R.S., Palmiter, R.D., Dymecki, S.M., Moore, H., and Ansorge, M.S. (2015). Activity of Raphé serotonergic neurons controls emotional behaviors. Cell Rep. *13*, 1965–1976.

Tsutsui-Kimura, I., Natsubori, A., Mori, M., Kobayashi, K., Drew, M.R., de Kerchove d'Exaerde, A., Mimura, M., and Tanaka, K.F. (2017). Distinct roles of ventromedial versus ventrolateral striatal medium spiny neurons in reward-oriented behavior. Curr. Biol. *27*, 3042–3048.e4.

Vertes, R.P., Linley, S.B., and Hoover, W.B. (2010). Pattern of distribution of serotonergic fibers to the thalamus of the rat. Brain Struct. Funct. *215*, 1–28.

Watanabe, M., Sugiura, Y., Sugiyama, E., Narita, M., Navratilova, E., Kondo, T., Uchiyama, N., Yamanaka, A., Kuzumaki, N., Porreca, F., et al. (2018). Extracellular N-acetylaspartylglutamate released in the nucleus accumbens modulates the pain sensation: analysis using a microdialysis/mass spectrometry integrated system. Mol. Pain *14*, 1–10.

Wise, R.A. (2004). Dopamine, learning and motivation. Nat. Rev. Neurosci. *5*, 483–494.

Young, S.N. (2013). Acute tryptophan depletion in humans: a review of theoretical, practical and ethical aspects. J. Psychiatry Neurosci. *38*, 294–305.

Yuen, E.Y., Qin, L., Wei, J., Liu, W., Liu, A., and Yan, Z. (2014). Synergistic regulation of glutamatergic transmission by serotonin and norepinephrine reuptake inhibitors in prefrontal cortical neurons. J. Biol. Chem. *289*, 25177–25185.

ISCI, Volume *20*

Supplemental Information

Detection of a High-Turnover Serotonin Circuit in the Mouse Brain Using Mass Spectrometry Imaging

Eiji Sugiyama, Matteo M. Guerrini, Kurara Honda, Yuko Hattori, Manabu Abe, Patrik Källback, Per E. Andrén, Kenji F. Tanaka, Mitsutoshi Setou, Sidonia Fagarasan, Makoto Suematsu, and Yuki Sugiura

Contents

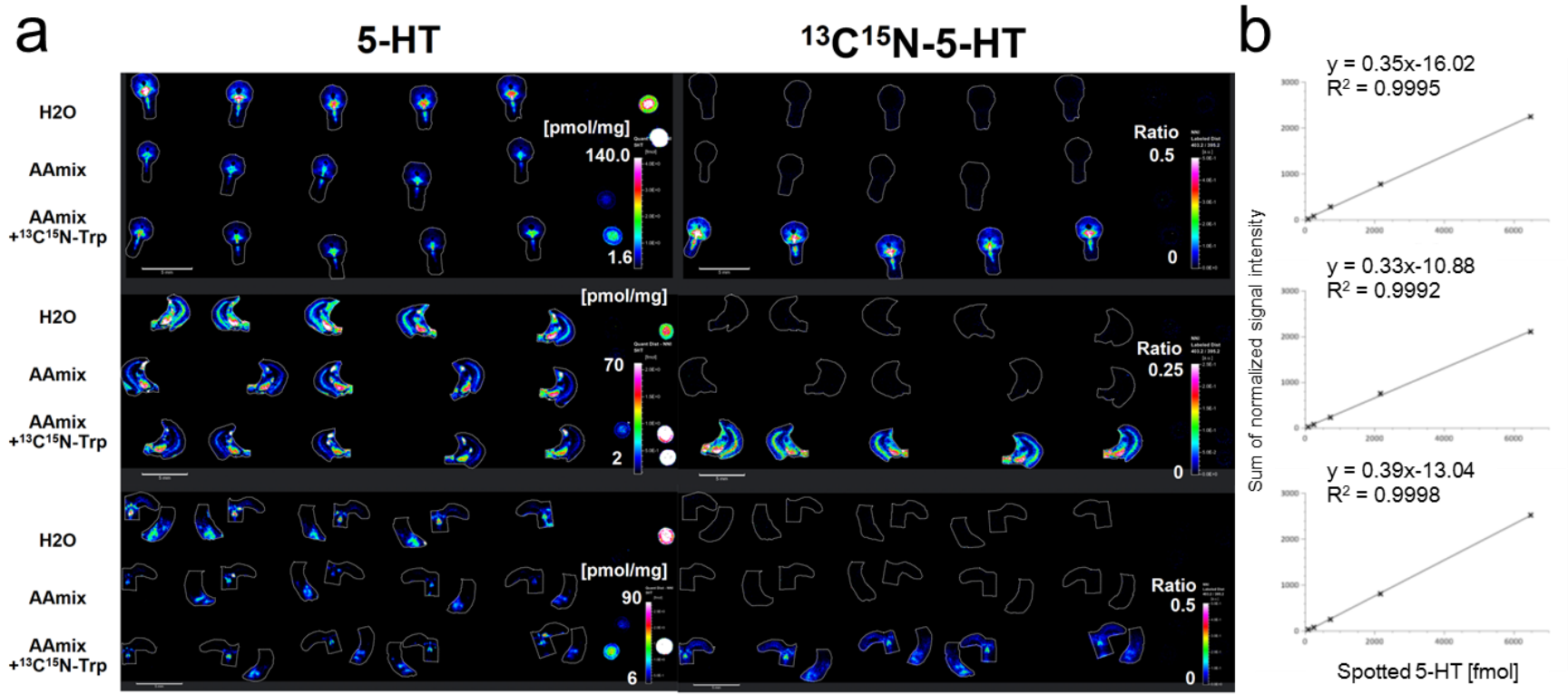

Figure S1. Distribution of 5-HT and $^{13}C^{15}N$-5HT used for the analysis of the ATD model, Related to Figure 5.

All the ion images used for the bars in **Figure 5E** were shown. The left (for 5HT-DPP) and the right (for $^{13}C^{15}N$-5HT-DPP) were obtained from the same mass spectra. Color scales show pmol/mg tissue for 5HT-DPP and relative intensity normalized by D_4-5HT-DPP for $^{13}C^{15}N$-5HT-DPP. **(b)** Calibration curves used for quantifying amount of 5-HT in site 1 (top), site 2 (middle), and site 3 (bottom). The data were obtained by the FT-ICR mass spectrometer.

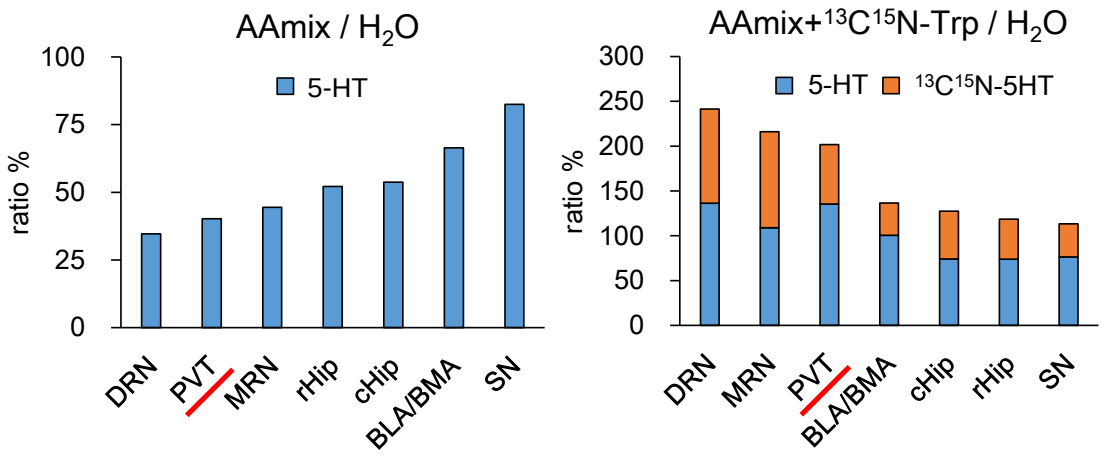

Figure S2. Relative concentrations of 5-HT in the brain nuclei, Related to Figure 5.

Left, relative levels of 5-HT in brain nuclei of the BALB/c male mice orally administrated with the AAmix normalized on the same nuclei of the group orally administrated with H_2O; **Right**, relative levels of 5-HT in brain nuclei of the mice orally administrated with the AAmix+$^{13}C^{15}N$-Trp group normalized on the same nuclei of the group orally administrated with AAmix only. The data were obtained by the FT-ICR mass spectrometer.

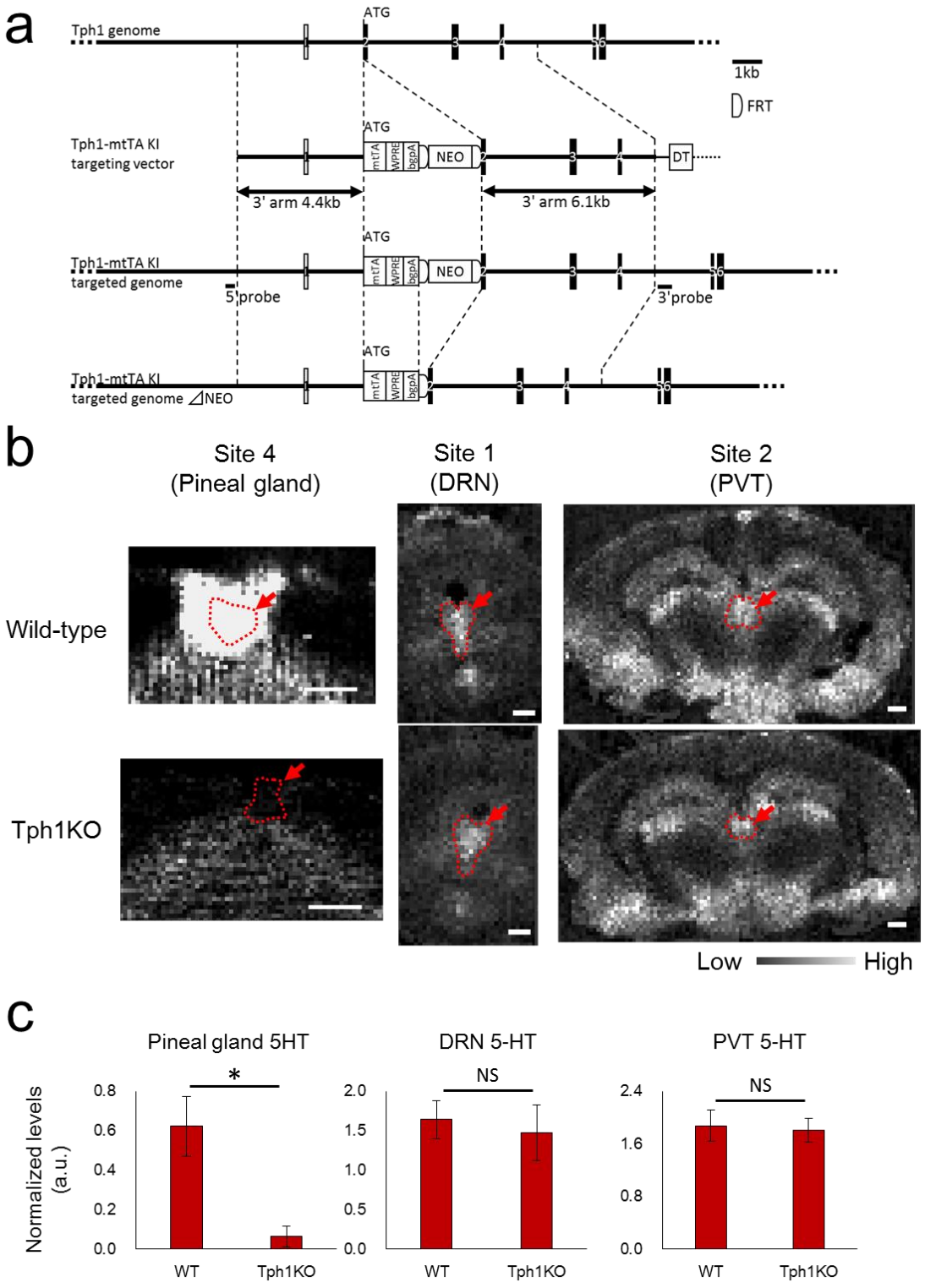

Figure S3. Disruption of TPH1 does not affect 5-HT levels in PVT, Related to Figure 5.

(a) Construction of Tph1-mtTA knock-in targeting vector. **(b)** Distribution of 5-HT in the three slices containing the pineal gland, DRN, or PVT. The regions were indicated by red arrows. The

area of the pineal gland was identified with H&E stain for a consecutive section. In wild-type, 5-HT was intensely detected from pineal gland as well as lumen of blood vessels. Scale bar = 500 μm. (**c)** 5-HT levels in the three regions. Data are shown in mean ± SD (n = 5 wild-type male and female mice at 8 weeks old and n = 3 Tph1-knockout male and female mice at 8 weeks old for the pineal gland, n = 4 male and female mice at 8 weeks old per group for the DRN, and n = 5 male and female mice at 8 weeks old per group for the PVT). NS: not significant ($P > 0.05$); *: $P < 0.05$ (Welch's t test). The data were obtained by the LIT mass spectrometer.

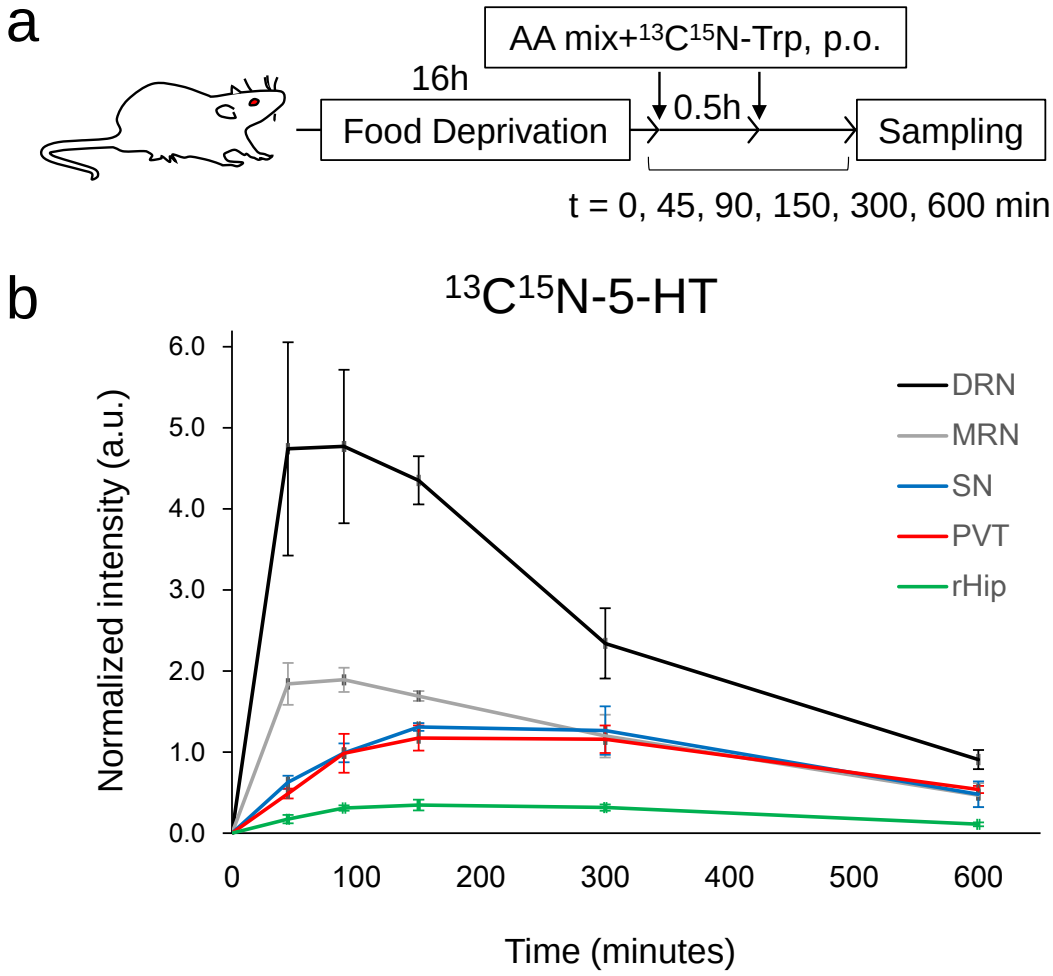

Figure S4. Levels of $^{13}C^{15}N$-5-HT in the brain of the ATD mice, Related to Figure 5.

Time course of newly-synthesized 5-HT in the indicated brain regions. (**a)** Schematics of the experimental procedure. After 16 h of food depletion, the BALB/c male mice at 10-11 weeks old were orally administered the AAmix+$^{13}C^{15}N$-Trp at t = 0 h and t = 0.5 h. Sampling of the brain was performed at the indicated time points. (**b)** Levels of newly-synthesized 5-HT ($^{13}C^{15}N$-5-HT) in the indicated brain regions. Black, white, blue, red, green lines connect the mean levels of $^{13}C^{15}N$-5-HT in the DRN, MRN, SN, PVT, and rHip at the indicated times. Error bars show SD (n = 4 mice). The data were obtained by the LIT mass spectrometer.

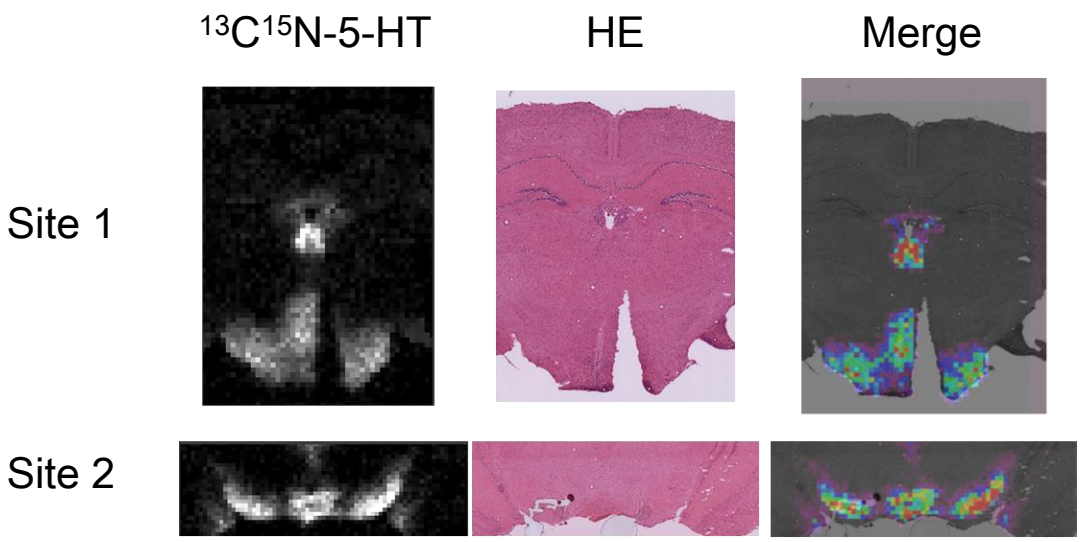

Figure S5. Preferential delivery of newly synthesized $^{13}C^{15}N$-5-HT from the DRN and MRN to the PVT and SN, Related to Figure 6.

Images of $^{13}C^{15}N$-5-HT, HE staining, and the merged are shown in left, center, right, respectively. The data were obtained by the LIT mass spectrometer.

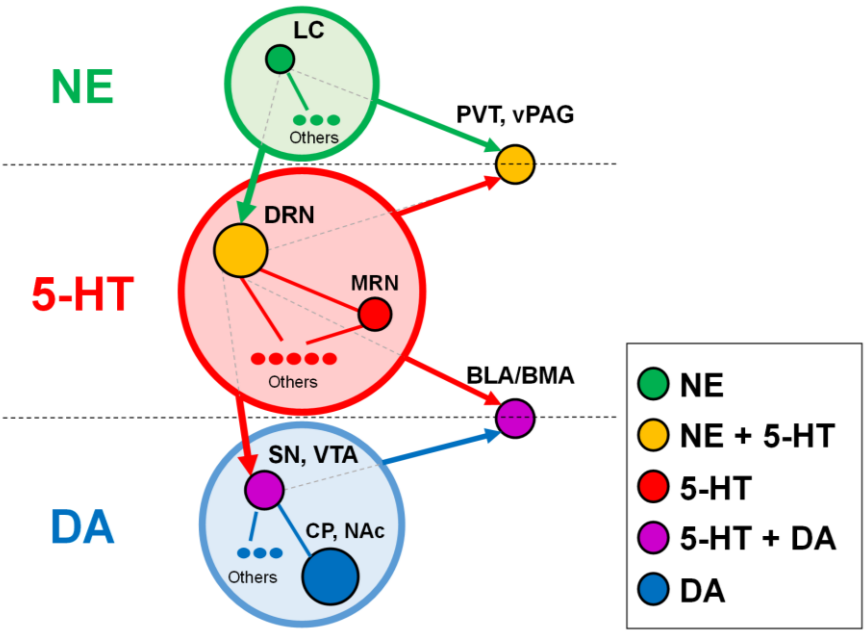

Figure S6. Schematic illustration of the monoaminergic main pathways based on levels of the monoamines, Related to Figure 2.

BLA/BMA: basolateral/ basomedial amygdala, CP: caudate-putamen; DRN: dorsal raphe nucleus, LC: locus coeruleus; MRN: median raphe nucleus, NAc: nucleus accumbens; PVT: paraventricular nucleus of the thalamus, SN: substantia nigra, vPAG: periaqueductal gray, ventral part; VTA: ventral tagmental area.

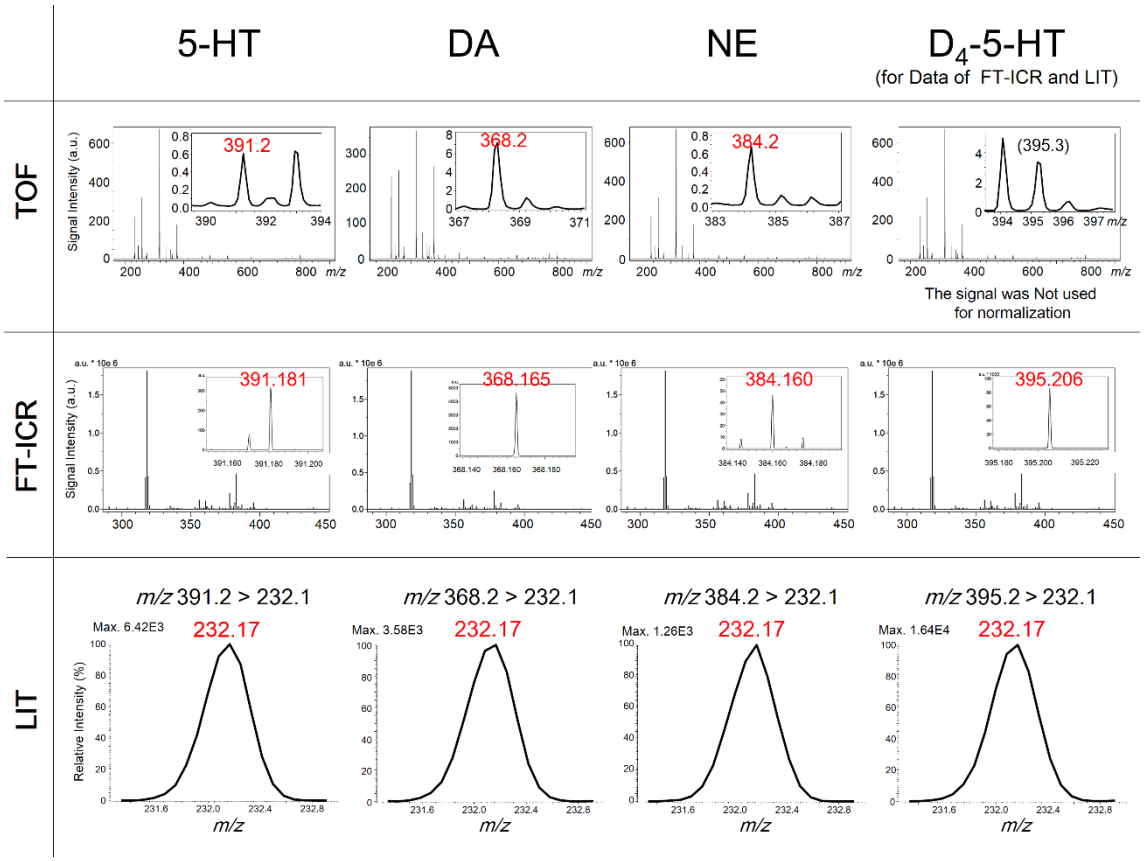

Figure S7. Mass spectra including target signals obtained by the 3 types of mass spectrometers, Related to Figure 1.

Representative mass spectra obtained with the TOF (top), the FT-ICR (middle), and the LIT (bottom) mass spectrometer are shown. Spectra for 5-HT, NE, and D_4-5-HT were obtained from the paraventricular nucleus of the thalamus, while the spectra for DA were obtained from the caudate putamen. Note that signal derived from D_4-5-HT was used as internal standard for not TOF but FT-ICR and LIT. The TOF data were normalized with TIC and the signal intensity from standard spots of 5-HT.

Transparent Methods

Chemicals

We obtained D_4-5HT creatinine sulfate complex from IsoSciences (PA, USA), tetrafluoroborate salts of 2,4-diphenyl-pyrylium (DPP) from Sigma-Aldrich (MO, USA), 2,5-dihydroxybenzoic acid (DHB) from Bruker Daltonics (MA, USA), $^{13}C_{11}{}^{15}N_2$-Tryptophan (^{13}C 97%, ^{15}N 95%) ($^{13}C^{15}N$-Trp) from Taiyo Nippon Sanso (Tokyo, Japan).

Mice

C57BL/6J male or BALB/cByJ male mice at 8-12 weeks old were purchased from Japan SLC (Hamamatsu, Japan) or CLEA Japan (Tokyo, Japan). All animal experimental procedures were approved by the Experimental Animal Committee of the Hamamatsu University School of Medicine and Keio University School of Medicine. After cervical dislocation euthanasia, the brains of the mice were isolated and immediately frozen in powder dry ice and then stored at −80°C. ATD model was prepared according to a protocol used in previous studies (Biskup et al., 2012). Briefly, after a food depletion for 16 h, the BALB/c male mice at 10-11 weeks were treated by gavage with amino acid mixture (AAmix), AAmix with labeled tryptophan (AAmix+$^{13}C^{15}N$-Trp) or water two times with an interval for 30 min. The mice were killed to obtain blood and brain after 150 min of the initial gavage. The brains were collected as described above, and the whole bloods were immediately collected from the hearts and then frozen with powdered dry ice. For time course analysis, brains of the BALB/c male mice at 10-11 weeks belonging to the group of AAmix+$^{13}C^{15}N$-Trp were collected at 0, 45, 90, 150, 300, 600 min. We allocated the mice randomly into experimental groups, and we did not use masking during data collection and data analysis.

Infusion of $^{13}C^{15}N$-Trp into DRN and MRN was performed as follows: the BALB/c male mice at 12 weeks were anesthetized with 2% isoflurane and were implanted stereotaxically with a guide cannula (CXG-4, Eicom, Kyoto, Japan) directed between DRN and MRN the prefrontal cortex (AP −4.5 mm, ML –0.0 mm, DV –3.0 mm from the bregma). Cannula was inserted with a 10° angle to avoid damage to the superior sagittal sinus. The guide cannula was immobilized with dental acrylic and filled with a dummy cannula (CXD-4). After the surgery, the mice were housed individually for at least 1 week before the following infusion. After infusing $^{13}C^{15}N$-Trp 50 mM, diluted in Ringer's solution (147 mM Na^+, 4.0 mM K^+, 2.3 mM Ca^{2+} and 156 mM Cl^-) by use of an injection cannula (CX) and a microinfusion pump (Fusion 100T, Chemyx, TX, USA) with a gas-tight syringe at a rate of 0.05 µL/min, mice were immediately anesthetized with isoflurane and the brains were collected.

We used male and female TPH1-deficient mice at 8 weeks old, which are the Tph1-mammalianized tTA (mtTA) homozygotes prepared as follows. A C57BL/6 BAC genomic clone RP23–4G4, which contains the Tph1 gene, was isolated from a RP23 mouse genomic BAC library

(Advanced GenoTechs, Tsukuba, Japan). The Quick and Easy BAC Modification Kit (Gene Bridges) was used for vector construction. We designed a gene-targeting vector in which the mtTA gene was placed just behind the translation initiation site of the Tph1 gene in frame (**Figure. S3**). Fragments of the mtTA coding sequence, woodchuck hepatitis virus posttranscriptional regulatory element (WPRE) and rabbit beta-globin poly(A) were ligated into pDTMC/FRTpgkgb2Neo (modified from pgkgb2Neo; Gene Bridges) containing a pgk/gb2–Neo cassette flanked by two *frt* sequences. This construct was used as the PCR template for the amplification of the fragment composed of the mtTA–Neo cassette. By using two primers, mtTA_KI_arm_F (5'-GTTCTGTGCTTAGCACTCATTTATCTGAACTTTCACACTTCAGATTCACCATGGCTCGCCTGGACAAGTC-3') and mtTA_KI_arm_R (5'-CTTTCGGAGGAATGGTCTTTGTTCTCTTTGTTCTCCTTGTTGTCTTCAATCACTATAGGGCTCGAGGAAG-3'), the cassette attached by 5' and 3' homology arms was amplified by PCR and then recombined into the translation initiation site of the Tph1 gene in RP23–4G4. The 10.5 kb fragment containing the exon 2–4 of the Tph1 gene and the iCre–Neo cassette was subcloned into pDT–MC#3 vector, including an MC1-promoter-driven diphtheria toxin gene. The resulting construct contained the translation initiation site of the Tph1 gene inserted by the mtTA–Neo cassette, 4.4 kb upstream and 6.1 kb downstream genomic sequences, and 4.4 kb pDT–MC#3. We introduced the linearized gene-targeting vector into the C57BL/6N-derived ES line RENKA (Mishina and Sakimura, 2007) and then selected recombinant clones under the medium containing 175 μg/mL G418. . The targeted clones were confirmed by Southern blot analysis and microinjected into eight-cell-stage embryos of a CD-1 mouse strain. The resulting chimeric embryos were developed to the blastocyst stage by incubation for ~24 h and then transferred to a pseudopregnant CD-1 mouse uterus. Germ-line chimeras were crossed with C57BL/6N female mice to establish the Tph1-mtTA mouse line.

Sample preparation for MALDI-MSI

Two male mouse brains were homogenized and frozen with an embedding dish at −80°C. The homogenate block or a whole brain was hold on a disc with an embedding medium (Super Cryoembedding Medium, SECTION-LAB, Hiroshima, Japan) and equilibrated at −16°C in cryostats (Leica Biosystems, Nussloch, Germany). Tissues were sectioned at 8-μm thick and thaw-mounted on a conductive indium-tin-oxide (ITO)-coated glass slides (Matsunami Glass Industries, Osaka, Japan). We spotted a blank and 5HT solutions (0.4 μL/spot, 0.2 to 16.2 μM with a dilution factor of 3, dissolved in 50% methanol) onto the homogenate sections and then sprayed D_4-5HT solution (10 μM in 50% methanol) on the sections as an internal standard (IS) with an automated sprayer, which is a TM-Sprayer (HTX Technologies, NC, USA) or a SunCollect

(SunChrom, Friedrichsdorf, Germany). The parameters for TM-Sprayer were set as follows: spray gas flow at 10 psi, nozzle temperature at 80°C, the number of spray cycles at 12, the speed of the nozzle movement at 1200 mm/min, and flow rate at 40 µL/min. The parameters for SunCollect were set as follows: spray gas flow at 29 psi, nozzle temperature at room temperature, the number of spray cycles at 10, the speed of the nozzle movement at 1000 mm/min, and flow rate at 20 µL/min. To perform on-tissue derivatization of monoamines, the DPP solution (1.3 mg/mL in methanol) was manually sprayed using an airbrush (Procon Boy FWA platinum; Mr. Hobby, Tokyo). The manual spray was performed at room temperature with 40 µL/mm^2 and a distance of approximately 50 mm. The DHB solution (40 mg/mL in 50% methanol) was sprayed on the sections in the same manner as that for the IS. DHB solution (40 mg/mL in 50% methanol) was sprayed on the sections by the same way for the IS.

MALDI-MSI

The samples were measured by a time-of-flight (TOF) type mass spectrumeter (ultrafleXtreme, Bruker Daltonics) or a MALDI-Fourier transformation ion cyclotron resonance (FT-ICR) mass spectrometer (solariX XR 7T, Bruker Daltonics), or a linear ion trap (LIT) mass spectrometer (LTQ XL, Thermo Fishcer Scientific). We selected an optimal mass analyzer depending on the purpose of the experiments. Each instrument has functional differences in regard to data acquisition speed, signal sensitivity, and acquired data size, which limit the available data analysis software. Owing to its high-speed data acquisition, the TOF mass spectrometer was used for screening monoamine rich in regions from among the whole mouse brain sections (Figure 2a), although its sensitivity is lower than those of others because of insufficient mass resolution to resolve small signals (Figure S8). An instrument with a FT-ICR mass analyzer, which has greater mass resolution (Figure S8), thus, can detect trace signals and was therefore used for the selected brain slice measurement to reconstruct the three-dimensional model (Figure 2b and Video S1) and for quantitative comparison with the calibration curves (Figures 4, 5, and S1). The disadvantage of FT-ICR MS is its larger data size than others. The LIT mass spectrometer, which has higher sensitivity and selectivity due to its larger capacity for ion trapping and specific monitoring of fragment ions produced by tandem mass spectrometry, was used for other quantitative comparison. Its data size is much smaller than those of others (Figure S8), although the speed of data acquisition is slower. The raster scan pitch was set depending on the experiment from 30 to 150 µm. Data were acquired from *m*/*z* 160 to 920 (for TOF data) or *m*/*z* 286.65 to 450.00 (for FT-ICR data) in positive ion mode. For LIT data, signals of 5-HT-DPP (*m/z* 391 > 232), $^{13}C_{10}{}^{15}N_2$-5-HT-DPP ($^{13}C^{15}N$-5-HT-DPP, *m/z* 403 > 233), D_4-5-HT-DPP (*m/z* 395 > 232) were monitored with a precursor ion isolation width of *m/z* 1.0 and a normalized collision energy of 45%. Ion images were reconstructed with flexImaging 4.1 (Bruker Daltonics), msIQuant

2.0.1.14(Källback et al., 2016), ImageQuest 1.1.0 software (Thermo Fischer Scientific) for the TOF data, the FT-ICR data, and the LIT data, respectively. Ion intensities of target ions were normalized with total ion current (for the TOF data), or a signal intensity of D_4-5HT-DPP (a signal at *m/z* 395.20615 for the FT-ICR data, and the signal monitored in LIT data). To quantify 5HT content, calibration curve was made using the signal intensity ratio (5HT-DPP to D_4-5HT- DPP) derived from the spots. We subtracted the value of blank spot subtracted from the values of each area. Quantity of $^{13}C^{15}N$-5HT was estimated by calculating a ratio ($^{13}C^{15}N$-5HT-DPP to 5-HT-DPP). Three dimensional images and a movie was constructed using SCiLS lab Premium3D software (SCiLS GmbH, Bremen, Germany). After finishing the measurement, the sections were stained by H&E stain to annotate the regions.

Sample preparation for LC-ESI-MS/MS

We mixed the frozen sections or the bloods with methanol containing an internal standard (L-methionine sulfone). We then added ultrapure water and chloroform. The mixture was centrifuged at 20,400 ×g for 15 min at 4°C. After centrifugation, the upper phase was filtered using an ultrafiltration tube (Ultrafree-MC, UFC3 LCC NB, Human Metabolome Technologies). The filtrate was dried with a vacuum concentrator (miVac, Genevac, UK), and then dissolved with ultrapure water (100 µL for bloods, 20 µL for sections) and was analyzed by LC-MS/MS. The lower and intermediate phases were dried up and the protein amount was determined using a BCA Protein Assay Kit (TAKARA BIO, Shiga, Japan).

LC-ESI-MS/MS

The metabolites in the samples were separated on the Discovery HS F5-3 column (2.1 mm I.D. × 150 mm, 3 µm particle, Sigma-Aldrich), using a gradient program with 0.1% formic acid in water (mobile phase A) and 0.1% formic acid in acetonitrile (mobile phase B). The gradient was scheduled as follows: 0.0–2.0 min, 0% B; 2.0–5.0 min, linear gradient to 25% B; 5.0–11.0 min, linear gradient to 35% B; 11.0–15.0 min, linear gradient to 95% B; 15.0–20.0 min, 95% B; 20.0–20.1 min, linear gradient to 0% B; 20.1–25.0 min, 0% B. The flow rate was set at 250 µL/min. The column temperature was maintained at 40°C. Triple-quadrupole mass spectrometers equipped with an electrospray ionization (ESI) ion source was used in the positive ion mode (LCMS-8040 for the blood samples and LCMS-8060 for the brain sections, Shimadzu). The mass spectrometers were operated in multiple reaction monitoring (MRM) mode with the following ion transitions: tryptophan *m/z* 205.1 > 188.2; $^{13}C^{15}N$-Trp *m/z* 218.1 > 200.05; 5HT *m/z* 177.1 > 132.1; $^{13}C^{15}N$-5HT *m/z* 189.1 > 142.1; L-methionine sulfone; *m/z* 182.0 > 56.1.

Supplemental References

Biskup, C.S., Sánchez, C.L., Arrant, A., van Swearingen, A.E.D., Kuhn, C., and Zepf, F.D. (2012). Effects of acute tryptophan depletion on brain serotonin function and concentrations of dopamine and norepinephrine in C57BL/6J and BALB/cJ mice. PLoS One 7, 7–14.

Källback, P., Nilsson, A., Shariatgorji, M., and Andrén, P.E. (2016). MsIQuant - Quantitation Software for Mass Spectrometry Imaging Enabling Fast Access, Visualization, and Analysis of Large Data Sets. Anal. Chem. 88, 4346–4353.

Mishina, M., and Sakimura, K. (2007). Conditional gene targeting on the pure C57BL/6 genetic background. Neurosci. Res. 58, 105–112.